https://doi.org/10.5194/egusphere-2024-1789
Preprint. Discussion started: 22 July 2024

A climatological characterisation of North Atlantic winter jet streaks and their extremes

Mona Bukenberger[1], Lena Fasnacht[1], Stefan Rüdisühli[1], and Sebastian Schemm[1]
[1]Institute for Atmospheric and Climate Science, ETH Zurich, Zurich, Switzerland
Correspondence: mona.bukenberger@env.ethz.ch

Abstract. The jet stream is a hemispheric-wide mid-latitude band of westerly wind. Jet streaks, which are regions of enhanced wind speed within the jet stream, characterize it locally. Jet streaks are frequent upper-tropospheric flow features that accompany troughs and ridges and form in tandem with surface cyclones. Upper level divergence in their right entrance and left exit regions couples them to surface weather via vertical motion and are regions prone to precipitation formation, which feeds back on the strength of upper level divergence and wind speed via diabatic heat release. This reanalysis-based study presents a systematic characterisation of the life cycle of jet streaks and extreme jet streaks over the North Atlantic during winter, their occurrence during three different regimes of the eddy-driven jet, and their relation to Rossby wave breaking (RWB) from a PV gradient perspective. Extreme jet streaks are most frequent when the North Atlantic jet is in a zonal regime, while they are least common when the jet is in a poleward shifted regime. Maximum wind speed on average occurs on the 329 K isentrope and the peak intensity of jet streaks, defined as the maximum wind speed throughout their evolution scales with the strength of the PV gradient, with mean values of 2.4 PVU $(100\,\mathrm{km})^{-1}$ for wind speeds exceeding 100 m s^{-1}. The peak intensity of jet streaks also increases with their lifetime and extreme jet streaks exhibit a prolonged intensification period rather than increased deepening rates. A positive trend in jet streak intensity appears to be emerging since 1979, but decadal variability still dominates the 43-year time series. A self-organising map technique identifies typical Rossby wave patterns in which jet streaks reach peak intensity and their preferred location and orientation within the large-scale environment. In case of anticyclonic RWB, the jet streak sits upstream of the ridge axis, while in case of no RWB the jet streak is zonally oriented and locates slightly downstream of the ridge axis. In some cases the jet streak is found farther downstream of the ridge axis but surprisingly no well-marked cyclonic RWB is identified at maximum jet streak intensity. As expected, the presence of an extreme jet streak is associated with a meridionally aligned pair of surface cyclones. More specifically, a cyclone is located poleward of an anticyclone plus, in some cases, a mesoscale cyclone upstream of both, which is associated with intense precipitation. This motivates a detailed follow-up study on the relative roles of diabatic and adiabatic processes in the formation of extreme jet streaks.

https://doi.org/10.5194/egusphere-2024-1789
Preprint. Discussion started: 22 July 2024

1 Introduction

The jet stream is a band of enhanced westerly winds in the mid- and upper troposphere. It steers large-scale weather systems and influences daily-to-weekly weather patterns with its meanderings. This makes the jet an important and longstanding research entity (see Palmén and Newton (1969), Davies (1997) and Hartmann (2007) and references therein for a detailed review of early studies). Contemporary atmospheric dynamics distinguishes two primary types of jet streams based on their key driving mechanisms (Woollings et al., 2010; Hartmann, 2007; Li and Wettstein, 2012). The subtropical jet, which is also referred to as the shallow jet, arises from angular momentum conservation within the Hadley circulation which causes westerly acceleration of the poleward moving air in the upper branch of the Hadley cell (Eichelberger and Hartmann, 2007; Li and Wettstein, 2012). Eddy momentum flux convergence in turn drives the tropospheric-deep eddy-driven jet (Hoskins et al., 1983; Li and Wettstein, 2012). Over the North Atlantic, the two jets are typically well separated. The subtropical jet is located over North Africa, while the eddy-driven jet is situated over the principal oceanic storm track. This jet is centred over the US East Coast and the Gulf Stream sector of the Atlantic Ocean and extends towards the southern tip of Greenland and further downstream into Europe (Koch et al., 2006). A merging of the two jets is an exception, although it has been observed in the past (Harnik et al., 2014). The mean position of the eddy-driven jet is partly a result of the prevailing orientation of Rossby wave breaking (RWB) because cyclonic RWB pushes the jet equatorward, while anticyclonic RWB pushes the jet poleward. (Hoskins et al., 1983; Chang et al., 2002; Hartmann, 2007; Woollings et al., 2008, 2010; Rivière, 2011). Thus, periods with preferred cyclonic, anticyclonic, or combined RWB lead to the manifestation of preferred North Atlantic jet positions (Benedict et al., 2004; Woollings et al., 2008). These poleward, equatorward, and zonal jet regimes can be identified by statistical clustering methods (Woollings et al., 2010; Frame et al., 2011). The response of the North Atlantic jet stream to tropical Pacific sea surface temperatures, for example, is thus partly a result of a change in the preferred orientation of RWB (Schemm et al., 2018).

The jet stream is not a homogeneous wind band but has a substructure which is characterised by local regions with increased wind speed termed jet streaks (Palmén and Newton, 1969, p. 206). Jet streaks are ubiquitous features in the jet, locally modifying horizontal and vertical wind shear and couple to surface cyclones via transversal vertical motion in their entrance and exit regions. Jet streaks influence air travel times and safety (Karnauskas et al., 2015; Williams, 2016), because the strong horizontal and vertical shear in their vicinity can foster clear-air turbulence (Reiter and Nania, 1964; Williams and Joshi, 2013; Storer et al., 2017; Lane et al., 2012), which is expected to become more frequent and intense in a warming climate (Williams and Joshi, 2013; Storer et al., 2017; Williams, 2017). The accurate representation of jet streaks is also vital for reliable weather forecasting, as small-scale errors in these regions can quickly grow into large-scale forecast uncertainty (Gray et al., 2014; Saffin et al., 2017). Foundational studies linked jet streak dynamics to extratropical cyclogenesis and the release of convective instability. (Riehl, 1948; Beebe and Bates, 1955). Numerous studies have since investigated the link between jet streaks and surface weather events, such as explosive cyclogenesis (Riehl, 1948; Riehl and Sidney Teweles, 1953; Uccellini et al., 1984; Uccellini and Kocin, 1987; Velden and Mills, 1990; Clark et al., 2009), frontogenesis (Sanders and Bosart, 1985), severe precipitation (Riehl, 1948; Uccellini and Kocin, 1987; Armenakis and Nirupama, 2014), cold temperature extremes (Uccellini,

https://doi.org/10.5194/egusphere-2024-1789
Preprint. Discussion started: 22 July 2024

1977; Uccellini et al., 1984; Uccellini and Kocin, 1987; Armenakis and Nirupama, 2014; Winters, 2021), and extreme wind (Bluestein and Thomas, 1984; Wernli et al., 2002; Rose et al., 2004), too name only a few.

The relation between upper-level jet streaks and surface weather development is conveniently summarized in the conceptual four-quadrant-model (4Q-model), pioneered by Namias and Clapp (1949), Riehl and Sidney Teweles (1953) and Beebe and Bates (1955). In the 4Q-model, the flow is decomposed into geostrophic and ageostrophic wind components. In case of a straight jet streak, the acceleration of air parcels in the jet streak entrance imply poleward ageostrophic wind and horizontal divergence/convergence in the right/left entrance of the jet streak (Beebe and Bates, 1955; Cunningham and Keyser, 2000, 2004). This causes rising/sinking motion below the right/left entrance quadrants of the jet streak and vice versa for the jet exit, where equatorward ageostrophic wind prevails. Mass continuity then implies lifting and convergence beneath the right entrance and left exit quadrants of the jet streak. The former is part of a thermally direct transverse circulation in the jet entrance. Thermally indirect (Uccellini and Kocin, 1987) motion in the jet exit transports warm moist air into the left exit quadrant, where it undergoes lifting. This mechanism aids cyclogenesis and rapid intensification below the left exit quadrant of jet streaks, which fosters moist convection and thereby further lifting (Beebe and Bates, 1955). In an anticyclonically curved jet streak, quasi-geostrophic theory suggests that only lifting in the right jet entrance and sinking in the right exit prevail, while cyclonically curved jet streaks show only sinking in the left entrance and lifting in the right exit (Cunningham and Keyser, 2004; Clark et al., 2009). The 4Q-model has proven useful in numerous case studies (Uccellini, 1977; Uccellini et al., 1984; Sanders and Bosart, 1985; Uccellini and Kocin, 1987; Velden and Mills, 1990; Clark et al., 2009).

The potential vorticity (PV) perspective provides a powerful framework to study jet streaks due to (i) PV conservation under adiabatic flow (Ertel and Rossby, 1942) and (ii) the invertibility property (Hoskins et al., 1985), which allow to study the role of adiabatic and diabatic processes during the life cycle of jet streaks. The PV perspective has been employed to study the dynamics of extratropical cyclones and accompanying jet streaks (see, for example, Gyakum (1983); Boyle and Bosart (1986); Wernli et al. (2002); Binder et al. (2016); Martínez-Alvarado et al. (2016)) and specifically the influence of diabatic processes on extratropical cyclone dynamics (Hoskins et al., 1985; Hoskins and Berrisford, 1988; Davis and Emanuel, 1991; Grams et al., 2011; Schemm et al., 2013; Davies and Didone, 2013; Schemm and Wernli, 2014; Saffin et al., 2021; Attinger et al., 2021) including the formation of blocking (Pfahl et al., 2015; Steinfeld et al., 2020). Davies and Rossa (1998) established a quantitative link between isentropic wind speed and PV gradients and analyzed the dynamics of jet streaks, viewed as regions of enhanced PV gradients, as PV-frontogenesis under the assumption of adiabatic flow. Considering the utility of the PV gradient as a proxy for the jet, Bukenberger et al. (2023) expanded upon Davies and Rossa (1998) by using a three-dimensional Lagrangian PV gradient perspective to quantify the influence of diabatic processes on jet streak evolution. A key finding of Bukenberger et al. (2023) is the prominent role of diabatic PV gradient modification in case of strong jet streaks, which is consistent with the climatological study by Winters (2021) on extreme North Atlantic winter jet streaks. Regions of enhanced PV gradients are linked to Rossby waveguidability (Martius et al., 2010; Manola et al., 2013; Branstator and Teng, 2017; Wirth, 2020; Polster and Wirth, 2023), enabling the study of Rossby wave dynamics by means of the PV gradient perspective.

https://doi.org/10.5194/egusphere-2024-1789
Preprint. Discussion started: 22 July 2024

This study employs a PV gradient framework in conjunction with a jet streak identification and tracking algorithm and statistical clustering techniques to provide a comprehensive quantification of the life cycle properties of North Atlantic jet streaks. More specifically, the following research question are addressed

1. Is there a relationship between the intensity, lifetime and other characteristics such as their area, the maximum PV gradient, and isentropic level of jet streaks?
2. Is there an archetypal jet streak life cycle over the North Atlantic?
3. What is the large-scale flow situation as jet streaks reach their peak intensity?
4. What is the role of diabatic processes in jet streak evolution? Is it different for extreme vs. non-extreme jet streaks?

The methods to identify, track, and cluster jet streaks are presented in Sections 2.1.2 and 2.2. In Sect. 2.5, the fundamental link between isentropic PV gradient and horizontal wind speed is revisited. Section 3 presents the results, the core of which is a systematic composite study based on jet streaks clustered into different categories according to their large-scale dynamical environment in Sect. 3.4. Finally, we summarise our findings and provide an outlook to future research in Sect. 4.

2 Methods and Data

This study uses 6-hourly ERA5 data for the winter (DJF) period in the Northern Hemisphere between 1979 and 2023 interpolated in the horizontal on a 0.5° latitude-longitude grid (Hersbach and Bell, 2020; Hersbach et al., 2023). In the vertical, the data is interpolated onto 16 isentropic levels between 310 and 340 K in steps of 2 K.

To effectively use the PV gradient as a proxy for wind speed, theory requires a spatial lowpass filtering for both PV and wind data (Bukenberger et al., 2023). The here used low-pass filtering involves transforming the PV and wind fields into spherical harmonics space and applying a triangular truncation at spherical harmonics of degree 80. Instead of a sharp cutoff, we use a Gaussian decay to smoothly suppress modes of higher degree. More precisely, if the spherical expansion of the field is given by

$$f(\phi,\lambda) = \sum_{l=0}^{N} \sum_{m=-l}^{l} f_l^m Y_l^m(\phi,\lambda), \tag{1}$$

where $Y_l^m(\phi,\lambda)$ is the spherical harmonic of degree l and order m and f_l^m are the corresponding coefficients, the filtered field is

$$\tilde{f}(\phi,\lambda) = \sum_{l=0}^{N} e^{-(l/\sigma)^2} \sum_{m=-l}^{l} f_l^m Y_l^m(\phi,\lambda), \tag{2}$$

with $\sigma = 80$. The zonal wavenumber is m and the meridional wavenumber is $l-m$, thus, for a zonal wavenumber $m=0$ and $l=\sigma$ and the earth circumference $2\pi r_0 \approx 40{,}000\,\mathrm{km}$, this yields a meridional wavelength of approximately 500 km. Hence, the filtering gives only little weight to wavelengths smaller than 500 km but with no cut off. We refer to lowpass filtered wind as wind and lowpass filtered PV as PV from now on, unless stated otherwise.

https://doi.org/10.5194/egusphere-2024-1789
Preprint. Discussion started: 22 July 2024

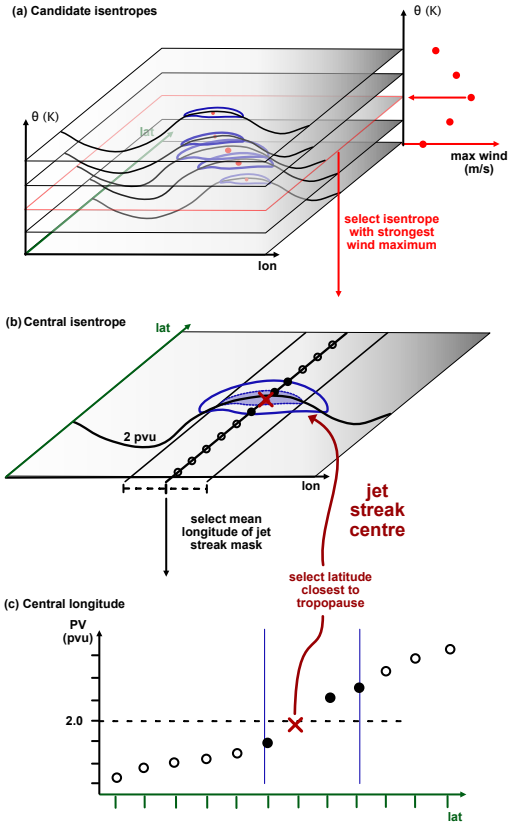

Figure 1. Schematic illustrating the jet streak centre identification algorithm. Panel (a) illustrates the identification of the central isentrope. The 2d-fields on different isentropes show the (black contours) 2 PVU isoline (with PVU being the unit of potential vorticity (PV), i.e., $1\,\mathrm{PVU} = 10^{-6}\mathrm{K}\cdot\mathrm{m}^2\mathrm{kg}^{-1}$) and the (blue contours) horizontal wind speed, 35 m s^{-1} isotach. The red circles on each isentrope indicate the position of wind speed maximum per isentrope. Scatters to the right show the (red dots) max wind on each isentrope and the red arrow points to the central jet streak isentrope. Panel (b) shows the calculation of central longitude. Contours show the same variables as in (a) on the central isentrope. The blue hashing masks the 99.25 percentile of instantaneous wind on the central isentrope, black lines surrounding blue hashing indicate the outermost longitudes of the 99.25 percentile wind speed mask and the black line in the middle of the blue hashing indicates the central longitude of 99.25 percentile wind mask. Panel (c) demonstrates the selection of the latitude closest to the tropopause on the central jet streak isentrope and longitude. It shows the (dashed line) 2 PVU isoline, the (blue vertical lines) outermost latitudes of 35 m s^{-1} wind speed mask on the central isentrope. Black markers show the PV at (open circles) each gridpoint on the central isentrope and longitude and PV (filled circles) on each gridpoint on the central isentrope and longitude for which wind speed exceeds 35 m s^{-1} and finally PV at (red cross) the jet streak centre.

https://doi.org/10.5194/egusphere-2024-1789
Preprint. Discussion started: 22 July 2024

2.1 Jet streak identification and tracking

To identify and track jet streaks, we use a time series of jet streak centre locations, $\mathbf{r_{js}}(t) = [\theta_{js}(t), \phi_{js}(t), \lambda_{js}(t)]^T$, where the isentrope $\theta_{js}(t)$ is the isentrope with maximal wind speed at time *t*. Further, $\phi_{js}(t)$ in degrees east is the jet streak centre longitude, and $\lambda_{js}(t)$ in degrees north is the latitude of the jet streak centre.

2.1.1 Identification

The algorithm to determine $\mathbf{r_{js}}(t)$ uses isentropic horizontal wind speed and PV. The three central steps of the algorithm, which are illustrated also in Fig. 1 are:

1. **Central isentrope.** The isentrope that exhibits maximum wind speed is identified (Fig. 1a). The search includes isentropes between 310 K and 340 K, with intervals of 2 K. The maximum wind speed is denoted jet streak intensity and the corresponding isentrope as the central isentrope.

2. **Central longitude.** First, a percentile threshold (99.25%) of the instantaneous wind speed on the central isentrope is used to create a coherent area of high wind speeds around the wind speed maximum. The median of the mask's longitudinal extent is defined as the central longitude (see Fig. 1b). If the wind speed maximum is positioned close to the boundary of the North Atlantic ($\pm 2.5^{\circ}$E), we compute the central longitude at this distance to the domain boundary[1].

3. **Central latitude.** The central latitude is the latitude with the minimum distance between the dynamical tropopause (2 PVU) and the PV at the location of the central longitude (see Fig. 1c). In the present implementation, we require the central latitude to lie at least within $\pm 5^{\circ}$N around the maximum wind along the central longitude.

Additionally, the jet streak centre is only accepted if the wind speeds is larger than 35 m s^{-1}. The projection onto the intersection with the tropopause in the last step is done to achieve tropopause-centred composites at a later stage.

The algorithm identifies exactly one jet streak centre within the North Atlantic domain per time step. In case of multiple jet streaks within the domain, it selects the most intense one. Hence, if a jet streak is missed, typically early in its life cycle, the algorithm accounts for it once it intensifies and eventually matures into the most intense jet streak in the North Atlantic sector. All weaker jet streaks are ignored. This implies that the mature phase of strong jet streaks is robustly captured, while results on the genesis and lysis phases must be interpreted more carefully.

2.1.2 Tracking

The zonal propagation speed of jet streaks exhibits only a weak case-to-case variability (Fig. 2). Roughly 70% of all six hourly distances between two consecutive time steps are within $4.5^{\circ}(6\,\mathrm{h})^{-1} \pm 7.5^{\circ}(6\,\mathrm{h})^{-1}$ or $[-3, +12]^{\circ}(6\,\mathrm{h})^{-1}$. Hence, two jet streak centres are linked to the same life cycle if the zonal distance between both can be covered by a zonal velocity from the above velocity range and within a time period of 24 h. A jet streak life cycle must have a minimum duration of 18 h (3 steps) and gaps of up to 24 h (4 steps) are allowed, whereby each fragment of the life cycle must be at least 6 h (1 step) long.

[1]The sensitivity to this choice was tested and is small. See limitations at the end

https://doi.org/10.5194/egusphere-2024-1789
Preprint. Discussion started: 22 July 2024

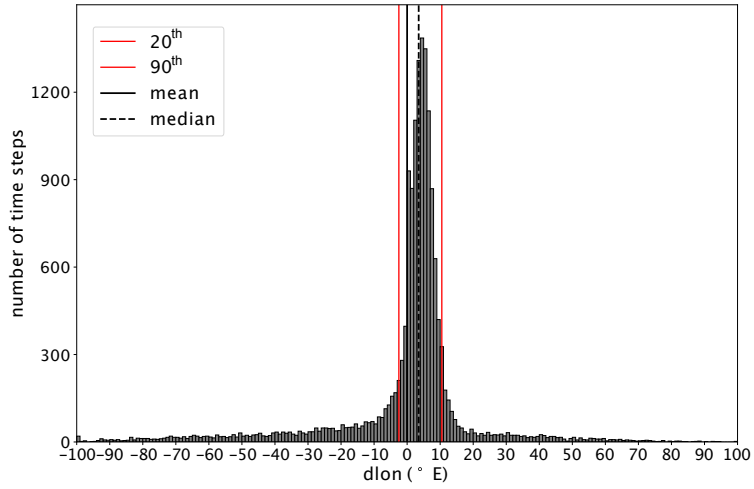

Figure 2. Histogramm of 6-hourly differences in longitudinal position of jet streak centers, calculated with the method detailed in Sect. 2.1.1. The vertical lines show the (black solid) mean, (black dashed) median, and 20th and 90th of 6-hourly differences in longitudinal position of jet streak centers.

2.1.3 Life cycle characteristic

After calculating jet streak centres for each time step and assigning event labels, characteristic properties of jet streak life cycles can be analyzed. To this end, the following definitions are used:

1. The first time step assigned to a jet streak event is called genesis.
2. The last time step assigned to a jet streak event is called the lysis.
3. The maximum jet streak intensity (i.e., maximum wind speed) during a jet streak event is defined as its peak intensity. The corresponding isentrope is used to compute the intensification rate throughout the life cycle.
4. The time between genesis and peak intensity is called intensification phase.

The identification of peak intensity and intensification is illustrated in Fig. 3c. The jet streak intensification rate is defined as the six hourly difference between the wind speed maxima in a jet streak object. It should be noted that the intensification rate is calculated on a fixed isentropic level, i.e. the isentropic level exhibiting the maximum wind speed throughout the entire life cycle and therefore denotes the acceleration of the wind at the level on which the maximum wind speed throughout the life cycle occurs. The maximum rate is denoted as the peak intensification rate.

https://doi.org/10.5194/egusphere-2024-1789
Preprint. Discussion started: 22 July 2024

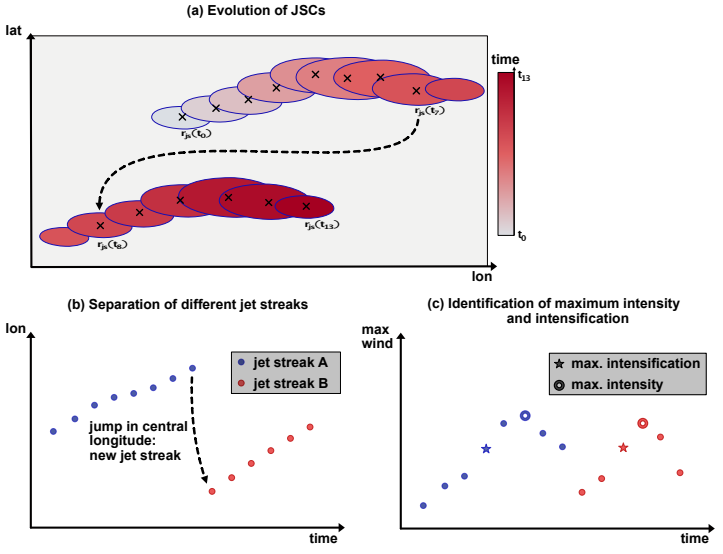

Schematic 3. Schematic illustrating the algorithms (a, b) tracking jet streak events and (c) identifying their times of strongest intensification and intensity. Panel (a) shows the (blue contours) wind speed on central isentropes for 14 consecutive time steps, 35 m^{-1}, the (black crosses) jet streak centres, and the (colours from white to red) time step. The dashed arrow indicates the longitudinal jump in the jet streak centre between end of first and beginning of second jet streak. Panel (b) shows jet streak centre longitude against time and jet streak centres of the (blue dots) first and second (red dots) jet streak (before longitudinal jump). Panel (c) shows the wind speed maximum on central isentrope against time for the wind speed maximum of (blue markers) first and (red markers) second jet streak. Stars and open circles indicate the time steps of peak jet streak intensification and intensity, respectively.

2.2 Clustering of jet streak events

2.2.1 Jet stream regimes

To establish the connection between jet streak life cycle characteristics and the state of the eddy-driven jet stream, we use a jet stream regime definition similar to that introduced by Frame et al. (2011). The regime definition relies on zonallay averaged but meridionally varying jet profiles, denoted as $U(t, \lambda)$, which are calculated by zonally and vertically averaging the zonal wind between 60°W and 0°W, and between the 700 hPa and 900 hPa. Next, a K-means clustering (Jain, 2010) with three degrees of freedom is applied to six hourly data. These clusters, which are denoted as S (Southern), M (Middle), and N (Northern), correspond to different states of the North Atlantic jet stream (Frame et al., 2011). Similar jet regimes for the North Atlantic (NA) jet stream have been identified in other studies, such as Woollings et al. (2010). Each jet streak time step can now be associated with one of the three regimes. Jet streaks that reach their peak intensity at a time associated with an S, M, or N regime are called S-, M-, or N-regime jet streaks, respectively.

https://doi.org/10.5194/egusphere-2024-1789
Preprint. Discussion started: 22 July 2024

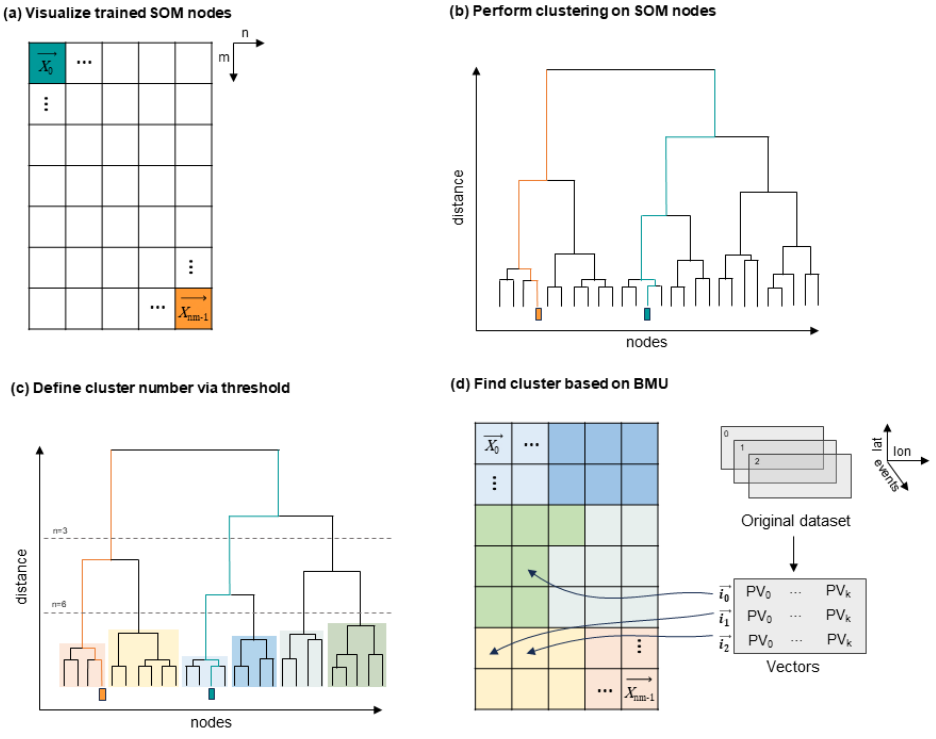

Figure 4. Visualisation of the clustering process: (a) 2d-SOM map generated through the algorithm's training with PV vectors from two different time steps, placing dissimilar nodes far away from each other; (b) The dendrogram, a visual result of hierarchical agglomerative clustering on the SOM nodes, groups those nodes and visualizes their merging pattern; (c) Altering thresholds of cophenetic distance produces various cluster numbers; (d) Assign each original PV vector to a reference vector of the SOM and thus to a cluster. Within each vector PV_0 is the normalized PV value on the first grid-point for the time step of maximum intensification and PV_k is the normalized PV value on the last grid-point for the time step of maximum speed.

2.2.2 SOM clustering

To classify the synoptic situations in which jet streaks intensify, the self-organizing map (SOM) method (Kohonen, 1995) is combined with agglomerative clustering. The SOM algorithm, based on an unsupervised neural network for clustering high-dimensional data, requires no prior knowledge of the resulting patterns, making it suitable for investigating synoptic circulation
175 clusters (Liu and Weisberg, 2011).

As illustrated in Fig. 4a, the SOM output is a two-dimensional $m \times n$ node map, with each node representing a reference vector and SOM nodes positioned in high-density regions of the input data space. Nodes closer together signify greater similarity (Hewitson and Crane, 2002). The map's shape determines the balance between accurately representing synoptic features (more nodes) a substantial reduction in dimensionality (fewer nodes).

https://doi.org/10.5194/egusphere-2024-1789
Preprint. Discussion started: 22 July 2024

The input data classifies upper-level jet streak dynamics based on isentropic PV fields. The central isentrope at peak jet streak intensity serves as the vertical level and PV fields at peak intensification and intensity as inputs. After remapping the jet streak center to (0.0°E, 0.0°N), PV fields are limited to $\phi \in [50°\mathrm{W}, 50°\mathrm{E}]$ and $\lambda \in [30°\mathrm{S}, 25°\mathrm{N}]$, then normalized to $[0, 1]$ using minimum-maximum scaling, before SOM clustering is performed. Several SOM sizes were tested, evaluating standard metrics like quantitative and topographical error. A 7×5 map was chosen to classify jet streak events (see Sect. D for details).

Hierarchical agglomerative clustering (Fig. 4b) further reduces the number of clusters. A dendrogram based on SOM nodes representing normalized PV maps serves as the basis. The dendrogram's y-axis indicates the within-cluster variance increase after merging clusters, visualizing cluster similarity and progressive merging via the default Ward-linkage algorithm. Nodes far apart on the SOM map exhibit large dendrogram distances. A distance threshold defines clusters, controlling maximum within-cluster variance (Gentleman, 2023) and the number/size of clusters. Lower thresholds yield more numerous, smaller, and more homogeneous clusters, while higher thresholds produce fewer, larger, and more heterogeneous clusters. The threshold balances two aims: keeping distinct synoptic patterns separate and isolating clusters with high fractions of extreme jet streak events. Through exploration a configuration of six clusters is identified for representing synoptic feature evolution between peak intensification and intensity assigns each jet streak event to one cluster based on its best-matching SOM unit. Composite analyses based on jet streak-centered fields are performed for each cluster (See Sect. 3).

2.3 Jet streak-centred composites

To obtain jet streak-centred composite, the input coordinate system is rotated to position the jet streak centre at the centre for each event and time step of interest using CDO's remapping function for regular grids (Schulzweida, 2023). A composite analysis utilising jet streak centre-centred fields for non-extreme and extreme jet streaks represents a significant component of the presented analysis. This analysis is employed to investigate the large-scale circulation patterns in which jet streaks evolve (Sect. 3).

2.4 Normalized jet streak occurence

To analyze the evolution and occurence frequency of jet streaks, we compute a normalized jet streak centre probability density function (PDF). It represents the likelihood of a jet streak centre to occur over a given region. The normalized PDF is obtained by fitting a Gaussian PDF to selected jet streak centres on the regular ERA5 grid to give equal weight to each event. Afterwards, the Guassian-smoothed field is divided by the total number of identified jet streaks. Finally, the field is weighted by the inverse area of each grid point. The integral of this field over the Earth's surface evaluates to one. This method ensures comparability of the normalized PDF between selected subsets of all jet streaks (e.g., non-extreme vs. extreme event climatologies).

2.5 A PV gradient perspective on jet streaks

PV on an isentropic surface is defined as

$$\mathrm{PV} = \frac{\zeta + f}{\sigma}, \tag{3}$$

https://doi.org/10.5194/egusphere-2024-1789
Preprint. Discussion started: 22 July 2024

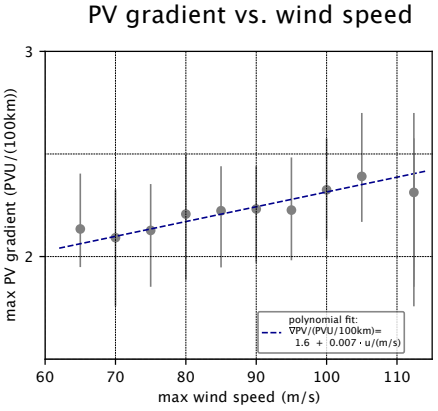

Figure 5. Relationship between the PV gradient at the jet streak centre and the maximum wind speed at the time of strongest jet streak intensity for. The blue dashed line shows a gaussian fit to a polynomial of first degree of the norm of PV gradient at jet streak centre depending on maximum wind speed, based on the 1120 times of peak jet streak intensity. The correlation between maximum wind speed and norm of PV gradient at jet streak centre for this time is 0.32. The position on the y-axis of each grey marker indicates the mean norm of the PV gradient at the jet streak centre for jet streaks with maximum wind speed within 2.5 m s^{-1} of its position on the x-axis. Each grey vertical bar spans the 20th–80th percentile of PV gradient at jet streak centre depending for jet streaks with maximum wind speed within 2.5 m s^{-1} of its position on the x-axis.

where ζ is the isentropic relative vorticity, $f = 2\Omega\sin(\phi)$ represents the Coriolis parameter, and the isentropic density $\sigma = -(1/g)\partial_\theta p$ is a measure of stratification. PV is given in units of $1\,\mathrm{PVU} = 10^{-6}\mathrm{K}\cdot\mathrm{m}^2\mathrm{kg}^{-1}$ throughout this work. As shown in Martius et al. (2010) and Bukenberger et al. (2023), the isentropic PV gradient ($\|\nabla_\theta \mathrm{PV}\|$) can be considered a proxy for the horizontal wind speed curvature under certain flow conditions, i.e.

$$\|\nabla_\theta \mathrm{PV}\| \approx -\frac{1}{\sigma_0} \triangle U, \tag{4}$$

where σ_0 is the isentropic density of the background flow and U is the horizontal wind speed. If variations in wind speed are dominated by a mode of wavelength λ, a direct proportionality between wind speed and PV gradient emerges:

$$\|\nabla_\theta \mathrm{PV}\| \approx \frac{4\pi^2}{\lambda^2\sigma_0} U. \tag{5}$$

In flow situations where Eq. (4) is a good approximation, the PV gradient serves as an analytical tool to connect jet streak evolution to diabatic processes. For wind speeds representing a superposition of multiple modes, shorter wavelengths dominate the curvature. Hence, the PV gradient is best used after applying a low-pass filter to PV and wind fields. The following paragraph presents the analytical approach and assumptions underlying the quantitative link between PV gradient and wind speed curvature insofar as they are important for the understanding of this study. A detailed version of the analysis can be found in Bukenberger et al. (2023). The basic idea is to consider a perturbation to a background flow characterised by constant wind, Coriolis parameter, and stratification.

https://doi.org/10.5194/egusphere-2024-1789
Preprint. Discussion started: 22 July 2024

Developing the Taylor polynomial of the PV gradient (Equation (4)) up to second order in perturbations that we assume to be much smaller than the background flow, and under the condition that variations in the perturbation of stratification are much smaller than wind speed curvature, i.e. for slowly varying stability and in case of large wind speed curvature common in jet streaks, the PV gradient is well approximated by

$$\|\nabla_\theta \mathrm{PV}\| \approx -\frac{1-\frac{\sigma'}{\sigma_0}}{\sigma_0} \triangle U. \tag{6}$$

Following an identical approach to the gradient of the logarithm of PV, $\|\nabla_\theta \ln(\mathrm{PV})\|$, which is also a good proxy for Rossby wave guidability (Polster and Wirth, 2023), yields – under the same conditions

$$\|\nabla_\theta \ln(\mathrm{PV})\| \approx -\frac{1-\frac{f'+\zeta'}{f_0}}{f_0} \triangle U. \tag{7}$$

If perturbations in stability are much smaller than the background stability, Eq. (6) simplifies to Eq. (4). In the case of small vorticity perturbations, Eq. (8) becomes

$$\|\nabla_\theta \ln(\mathrm{PV})\| \approx -\frac{1}{f_0} \triangle U. \tag{8}$$

Observations reveal a systematic stratospheric displacement of bands with high PV gradient compared to regions of maximum wind speed. This displacement is elucidated by the sharp increase in stability when transitioning from the tropospheric to the stratospheric side of the jet, leading to an increase in $1-\frac{\sigma'}{\sigma_0}$. The relationship between $\|\nabla_\theta \ln(\mathrm{PV})\|$ and wind speed curvature is less sensitive to perturbations in stability near the tropopause. If wind speed curvature is not too large, bands of high $|\nabla_\theta \ln(\mathrm{PV})|$ are well aligned with jet maxima. This makes $|\nabla_\theta \ln(\mathrm{PV})|$ a superior diagnostic for jet strength and waveguidability, as long as the jet is not excessively strong or narrow. For extreme jet streaks, often associated with bands of negative PV on the tropospheric side of the jet, the PV gradient becomes the superior diagnostic.

In flow situations in which Eq. (4) is a good approximation, which corresponds to balanced flow situations, the PV gradient serves as a proxy variable to connect jet streak evolution to diabatic processes. Although PV is materially conserved in adiabatic flow situations, the PV gradient can be modified by deformation and shear. A Lagrangian perspective on PV gradient evolution, disentangling diabatic from adiabatic contributions to changes in $\|\nabla_\theta(\mathrm{PV})\|$ as demonstrated in Bukenberger et al. (2023), offers a unique opportunity to quantify the influence of diabatic processes on upper-level jet dynamics.

Even if a direct link between PV gradients and wind speeds cannot be established, regions of high PV gradient still indicate significant variations in both wind and thermal stratification on tropopause-intersecting isentropic surfaces. This is particularly likely in flow situations far from geostrophic balance, such as those occurring in regions of enhanced diabatic activity or during strong jet streak intensification. In these situations, the PV gradient perspective remains meaningful for studying jet streak dynamics, especially when considering jet streaks in close connection to upper-level frontogenesis and changes in stratification.

Figure 5 illustrates the relationship between jet streak intensity and PV gradient at the jet streak centre at time of peak jet streak intensity. A linear fit describes this relationship. The correlation between maximum wind speed and PV gradient at jet streak centre at time of peak jet streak intensity is 0.32. Due to the considerable variability in jet streak width and tropopause

https://doi.org/10.5194/egusphere-2024-1789
Preprint. Discussion started: 22 July 2024

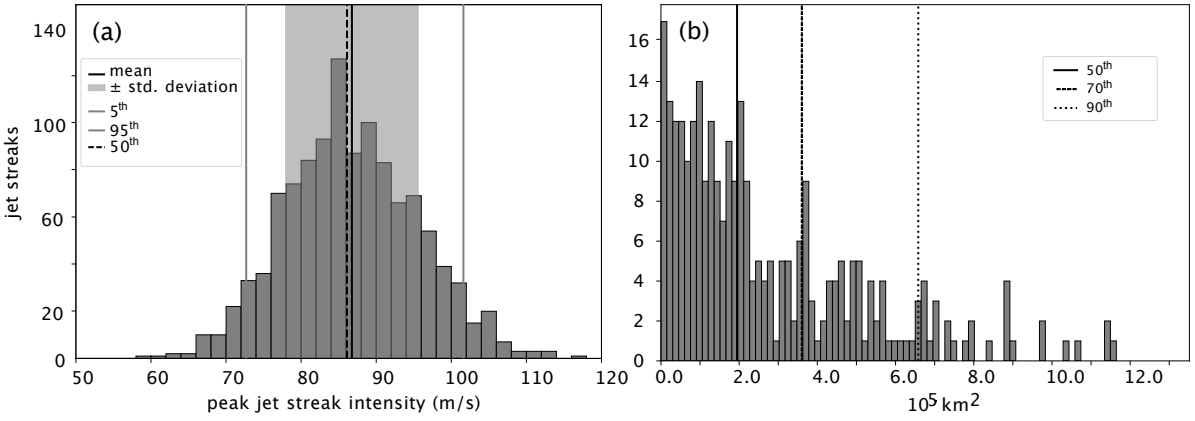

Figure 6. Jet streak characteristics at time of peak intensity. (a) Histogram of peak intensity for all 1120 jet streaks with a bin width of 2 m s^{-1}. Light-grey areas indicate the width of the standard deviation around the mean wind speed and black vertical lines the mean (thick solid), median (thick dashed), 5th percentile (thin grey solid) and 95th percentile (thin grey solid). (b) Histogram of extreme wind speed area at peak jet streak intensity for cases for which it is non-zero with a bin width of $0.15 \cdot 10^5$ km^2, with black vertical lines indicating the 50th (solid), 70th (dashed), and 90th (dotted) percentiles.

stability, the observed limited correlation and imperfect fit are expected. Despite these complicating factors, the PV gradient proves to be a reliable indicator of jet streak intensity. This analysis underscores the utility of the PV gradient framework for investigating jet streak dynamics. Notably, at the highest maximum wind speeds, exceeding 104 m s^{-1}, the PV gradient exhibits a slower growth with maximum wind speeds, potentially influenced by substantial stability variations across the tropopause in the most extreme jet streak cases.

3 Results

3.1 Characteristics of North Atlantic winter jet streaks

We begin with an examination of basic jet streak life cycle characteristics. The distribution of peak intensity of all 1120 jet streaks exhibits a nearly symmetric shape with a standard deviation of 8.8 m s^{-1} around a mean value of 86.7 m s^{-1} (solid black line and grey box in Fig. 6a). Closer inspectiona reveals a mild skew towards higher peak intensities. The median peak jet streak intensity is 86.1 m s^{-1}, while the 5th and 95th percentiles are 72.7 m s^{-1} and 101.6 m s^{-1}, respectively.

Relationship with jet regimes

We find some variations in jet streak characteristics between the three large-scale jet regimes of Frame et al. (2011). The M-regime jet streak distribution, comprising 520 jet streak maxima, exhibits increased variability and slightly higher peak intensities compared to the total climatology. The N regime, involving 295 jet streaks, features weaker jet streaks and smaller

https://doi.org/10.5194/egusphere-2024-1789
Preprint. Discussion started: 22 July 2024

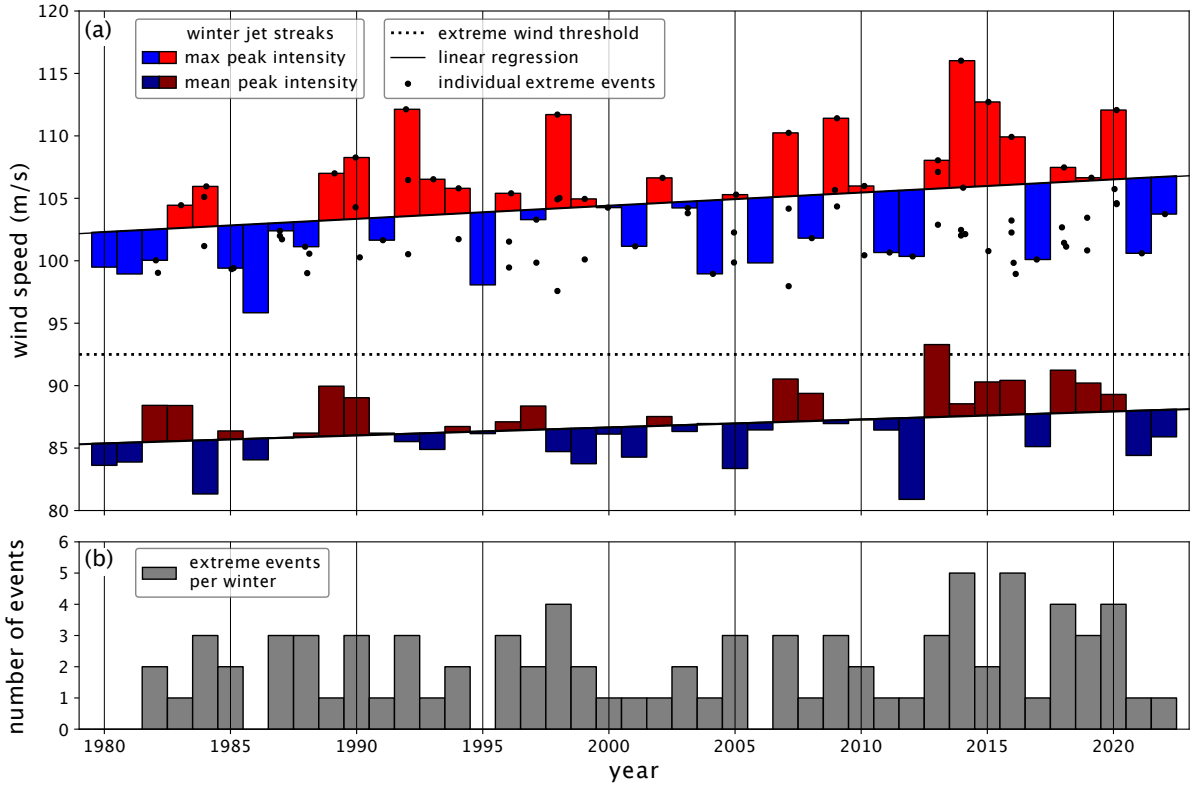

Figure 7. Temporal evolution of North Atlantic winter (extreme) jet streaks. (a) Mean and maximum peak North Atlantic winter jet streak intensity. Black dots: individual extreme jet streak events. The dotted line indicates the threshold for extreme wind speeds at 92.5 m s^{-1}. Dark red and dark blue bars indicate winter means of peak jet streak intensities (m s^{-1}), with red or blue bars plotted according to whether they are above or below the least squares fit linear regression for the period 1979–2023. Light red and blue bars indicate winter maxima of peak jet streak intensities (m s^{-1}), i.e. the peak intensity of the strongest jet streak event of each year. (b) Yearly number of extreme events per winter across ERA5 time span. Grey bars: Number of extreme jet streak events per winter.

Regime	Events	Mean	±	5th	50th	95th
		m s^{-1}	m s^{-1}	m s^{-1}	m s^{-1}	m s^{-1}
All	1147	86.1	8.8	72.7	86.7	101.6
S	520	85.7	8.4	73.6	86.4	100.5
M	295	88.1	9.0	72.9	88.5	104.3
N	295	84.2	8.2	71.6	84.1	96.9

Table 1. Characteristic properties of the distribution of peak jet streak intensity, for all jet streaks and jet streaks reaching their peak intensity in an S, M or N regime. Shown are the mean, the standard deviation (±),5th, 50th, and 95th percentile of peak jet streak intensity.

https://doi.org/10.5194/egusphere-2024-1789
Preprint. Discussion started: 22 July 2024

variability, and the distribution of S-regime jet streak maxima closely mirrors the overall climatology but displays decreased variability (Tab. 1). The results of stronger upper-level jet streak intensity for M-regime jets align with the findings of Frame et al. (2011) and Woollings et al. (2010), who showed that M-regime jets skew towards higher wind speeds compared to those in the S and N regimes. Figure 6b shows the distribution of extreme wind speed area at time of peak intensity on the central isentrope for the 293 jet streaks for which peak intensities exceed 92.5 m s^{-1}. Of those, 64 are S-, 173 are M-, and 44 are N-regime jet streaks. The 50th percentile of extreme wind speed area for those jet streaks is $1.95 \cdot 10^5$km^2, while the 70th and 90th percentiles are $3.58 \cdot 10^5$km^2 and $6.58 \cdot 10^5$km^2, respectively. We define extreme jet streaks as those events for which the area on which wind speeds exceed 92.5 m s^{-1} is larger than $3.58 \cdot 10^5$km^2 at time of their peak intensity, a definition yielding 85 extreme events.

Variability and trends (1979—2023)

Figure 7 shows the evolution of the winter mean and maximum peak jet streak intensities over DJF 1979–2023 in ERA5. The winter-mean peak jet streak intensity (dark red and blue bars) shows an increase at a rate of 0.064 m s^{-1}, starting at 85.3 m s^{-1} in 1979. The winter maximum peak jet streak intensity shows at trend of 0.11 m s^{-1}, starting at 102.2 m s^{-1} in 1979. Notably, seven of the ten strongest extreme jet streak events occurred after 2005. The number of extreme events per winter also shows an upward trend over the ERA5 period, although interannual and interdecadal variability are larger than the trend.

Both the winter-mean and winter maximum peak jet streak intensities show smaller trends than the interdecadal variability. The trend in the maximum peak jet streak intensity is almost twice as large as the trend in mean peak jet streak intensity. This is consistent with the findings of Shaw and Miyawaki (2023), who observed that extreme wind speeds are increasing at a faster rate than average wind speeds. Although this trend has not yet reached statistical significance, it is expected to do so by 2050. We also observe a correlation between the interannual variability of mean and maximum peak jet streak intensity. In winters with a mean jet streak intensity above the linear trend, the maximum jet streak intensity tends to show positive anomalies, and vice versa in winters with a mean below the trend.

Height of jet streaks at peak intensity

The distribution of θ_{peak} of all jet streaks (grey bars in Fig. 8) appears bimodal, with peaks at 328 K and 340 K. Jet streaks with high central isentropes tend to be more southerly and weaker than the average jet streak, suggesting that the maximum at high isentropes is due to shallow subtropical jet streaks (not shown). Second, while the set of all jet streaks has central isentropes down to 310 K, the minimum central isentrope for jet streaks with peak wind speeds above 92.5 m s^{-1}(dark red in Fig. 8) and for extreme jet streaks (light red in Fig. 8, wind speeds on the central isentrope exceeding 92.5 m s^{-1} on an area of at least $3.58 \cdot 10^5$ km^2) are higher than 310 K, at 318 K and 322 K, respectively. Furthermore, the mean central isentropes at time of peak jet intensity increase with jet streak intensity, reaching 330 K for jet streaks with extreme peak intensities and 331.5 K for extreme jet streaks. The trend towards higher central isentropes for more extreme jet streaks suggests the importance of thermodynamics and possibly diabatic processes in jet streak dynamics.

https://doi.org/10.5194/egusphere-2024-1789
Preprint. Discussion started: 22 July 2024

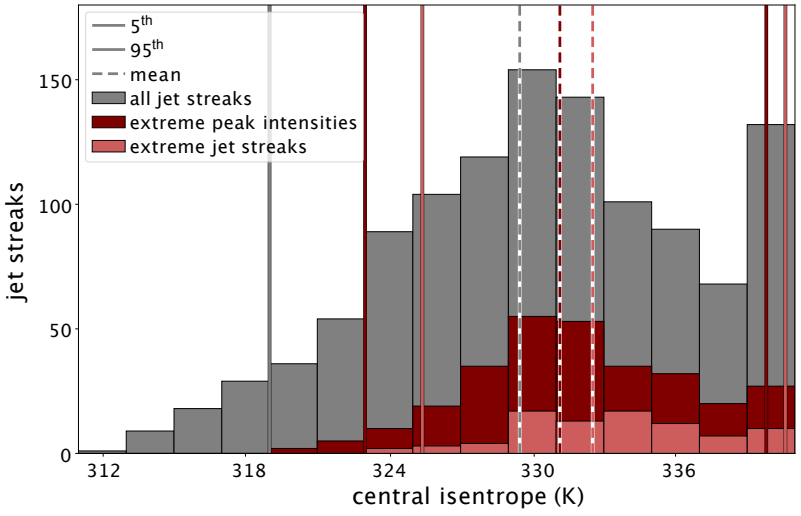

Figure 8. Histogram of central isentropes at peak jet streak intensity (θ_{peak}; K) for all jet streaks (grey), those with peak intensities above 92.5m s^{-1} (dark red), and extreme jet streaks (light red, wind speeds on the central isentrope exceeding 92.5 m s^{-1} on an area of at least 3.58·10^5 km^2), and vertical lines indicating the mean (dashed) and the 5th (solid) and 95th (solid) percentile of the distribution.

Jet streak lifetime and intensification phase

We proceed with the duration of different stages in jet streak evolution, examining climatologies of all and extreme jet streaks. Figure 9 presents the distributions of lifetimes for all, extreme, and selected subsets of all jet streaks selected based on the peak intensity. For all 1120 jet streaks (grey box and whiskers in Fig. 9a), the median and mean jet streak lifetimes are 48 h and 56 h, respectively. The 5th percentile (18 h) and 95th percentile distribution (114 h) together indicate substantial variability and a skew toward longer lifetimes. Stratifying the dataset based on jet streak intensity in Fig. 9a shows that the median and mean lifetime consistently increase with increasing peak intensity, as does its variability. The median lifetime is 24 h for jet streaks with peak intensity between 55 m s^{-1} and 65 m s^{-1} and reaches up to 66 h for jet streaks with peak intensity between 100 m s^{-1} and 110 m s^{-1}. Mean lifetimes are 12 h longer than medians for both groups. Despite a discernible trend toward longer lifetimes for more intense jet streaks, the median and mean lifetimes remain within the interquartile range of all jet streaks, for all subsets. The distribution of lifetimes for all jet streaks (Figure 9b) provides additional context to the correlation between jet streak lifetimes and peak intensities. It illustrates an exponential decrease in the occurrence as lifetimes increase. This figure also shows the mean and the 5th and 95th percentile of jet streak lifetime distributions for M-, N-, and S-regime jet streaks. The 5th percentiles is 18 h for jet streaks in all regimes and the mean lifetime of jet streaks in each regime remains within 2 h of the mean lifetime of all jet streaks. The 95th percentile of jet streak lifetimes is, at 120 h, half a day longer for S- than for N-regime jet streaks.

The insights from Fig. 9 suggest that the lifetime of jet streaks does not exhibit a strong dependency on the three jet stream regimes of Frame et al. (2011). Stronger jet streaks are long lived independent of the jet regime. However, while stratifying jet

https://doi.org/10.5194/egusphere-2024-1789
Preprint. Discussion started: 22 July 2024

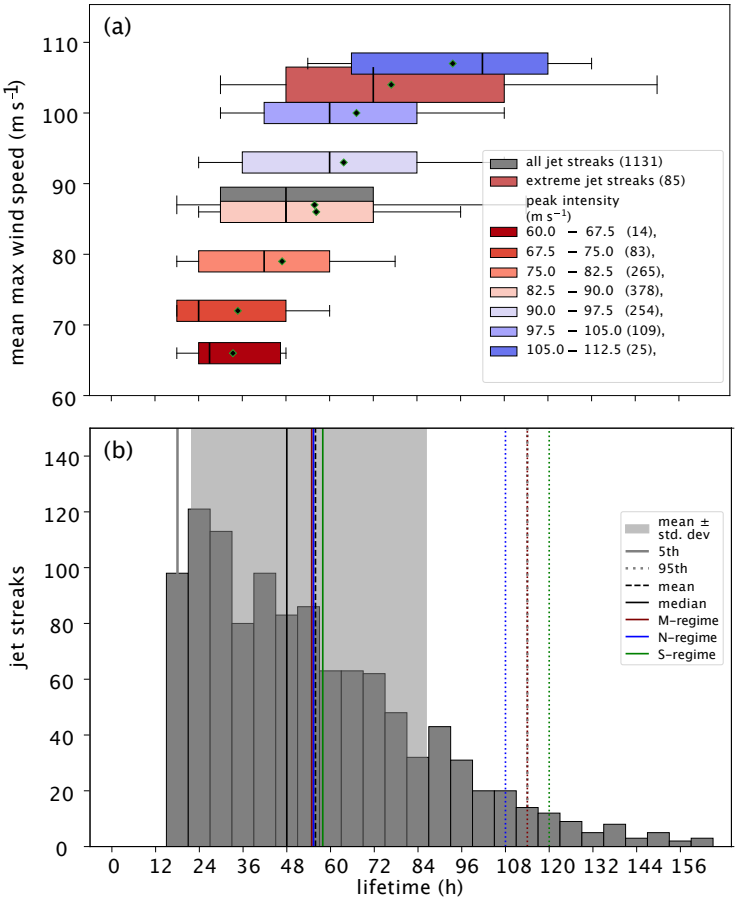

Figure 9. Analysis of jet streak lifetime. (a) Box-plots for lifetime stratified for peak jet streak intensity for (wide grey box) all jet streaks, (light red uppermost box) extreme jet streaks, and (dark red to dark blue) jet streaks with increasing peak intensities. The position on the y-axis indicates the mean peak intensity for all jet streaks of the respective category, and the width in y-direction is equal to the standard deviation. In the box plots, the left boundary of the box indicates the 25th, the black vertical line within the box the 50th, and the right boundary the 75th percentile. Whiskers to the left and right indicate the 5th and 95th percentile. The black square inside the box marks the mean of the distribution. (b) Histogram of jet streak lifetime for all jet streaks in dark grey bars, bins every 6 h, with the light grey area representing the width of the standard deviation around the mean lifetime, and vertical lines indicating the mean (black solid), 5th (left, grey solid), 50th (black dashed) and 95th (right, grey dotted) percentile of the lifetime distribution. Colored vertical lines indicate the mean (solid) and 95th percentile (dotted) of lifetimes for M- (red), N- (blue), and S-regime (green) jet streaks.

https://doi.org/10.5194/egusphere-2024-1789
Preprint. Discussion started: 22 July 2024

streaks by intensity reduces the variability in lifetimes somewhat for weak jet streaks, very intense jet streaks show particularly large variability, with interquartile ranges as large as the median lifetime. This hints at a substantial variability in the dynamics driving jet streak development, especially for strong jet streaks.

The average jet streak intensity at genesis is $73\pm$ 10.0 m s^{-1}. The average time between genesis and peak intensification amounts to 18 h (with a median of 6 h), and it takes on average 33 h (median 24 h) for jet streaks to reach their peak intensity (87 ± 9 m s^{-1}). Jet streaks last on average 57 h (median 48 h), and exhibit a mean intensity of 75 ± 11 m s^{-1} at their lysis, very close to the mean intensity at genesis. Note that in the mean, the intensification phase lasts about as long as the time between peak jet streak intensity and lysis. As for lifetime (Figure 9b), the duration of jet streak intensification and the time between peak jet streak intensity and lysis are heavily skewed toward longer time spans. The mean intensification phase lasts about 1.3 times as long for extreme, compared to all jet streaks, and the lifetime extreme jet streaks is on average 1.4 times as long.

For extreme jet streak, the mean intensity at genesis is 82 ± 13 m s^{-1}, 104 ± 9 m s^{-1} at peak intensity, and 83 ± 11 m s^{-1} at lysis. It is noteworthy that the distribution of the mean intensification rate of all jet streaks is failry similar to that of extreme jet streaks, with 0.55 ± 0.38 (m s^{-1}) h^{-1} for all and 0.62 ± 0.39 (m s^{-1}) h^{-1} for extreme jet streaks. The same holds true for the decay rate, with -0.65 ± 0.45 (m s^{-1}) h^{-1} for all and -0.79 ± 0.44 (m s^{-1}) h^{-1} for extreme jet streaks.

To summarize, the intensification rate does not determine whether a jet streak evolves into an extreme. Rather, it is the prolonged duration of the intensification period that is crucial. However, this result must be interpreted with caution, taking into account the large variability in intensification rates. It raises the question of what processes sustain the intensification period.

3.2 North Atlantic jet streak climatology

Examining the mean PV gradient and occurrence of extreme wind speeds based on low-pass filtered wind over the North Atlantic domain (Figure 10), we find 1405 time steps with extreme wind speeds over the North Atlantic in the winters 1979–2023 in the 6-hourly ERA5 data (Fig. 10a). Wind speeds above 92.5 $m\,s^{-1}$ occur over the eastern US, the Gulf Stream, Canada and from the Labrador Sea northeastward past Greenland downstream towards the UK. The highest frequencies form a southwest-to-northeast-oriented band centred over the western North Atlantic and extending into the central North Atlantic. This is in qualitative agreement with the regions in which Winters (2021) finds large frequencies of extreme winds.

The centres of extreme jet streaks at time of peak intensity (black dots in Fig. 10a) are mainly concentrated over the US East Coast - Gulf Stream sector. However, they also exhibit large variability, with some jet streaks reaching peak intensity over eastern North America or north of 55°N. Figure 10b shows the mean North Atlantic winter PV gradients and wind speeds. Key observations from the wind and jet streak climatologies are:

- Climatologically, highest mean PV gradients are found over the Great Plains. High wind speed and largest PV gradient are co-located at each longitude, but the PV gradient maximum is located upstream of the maximum wind speed and upstream of the region with highest jet streak density (black dots in Fig. 10a).

https://doi.org/10.5194/egusphere-2024-1789
Preprint. Discussion started: 22 July 2024

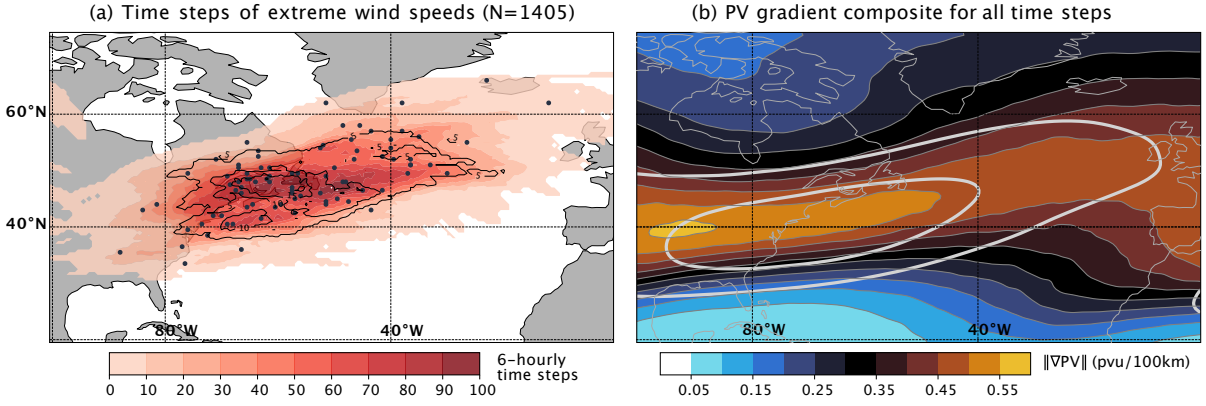

Figure 10. North Atlantic winter (DJF 1979–2020) climatologies based on 6-hourly ERA5 data. (a) Total number of 6-hourly time steps with extreme wind speeds on at least one isentrope over the North Atlantic domain (100°W–0°E × 20°N–75°N) in red colours. Contours show the number of peak jet streak intensity time steps for extreme jet streak events with extreme wind speeds on at least one isentrope over the North Atlantic domain, contours every 5 time steps. Jet streak centres of extreme jet streak events at time of peak intensity in black dots. (b) PV gradient climatology using 6-hourly ERA5 data at 329 K (the mean of all central isentropes at time of peak jet streak intensity) in colours. Thin grey contours: climatology of the PV gradient with contours every 0.1 PVU $(100\,\mathrm{km})^{-1}$, starting at 0.05 PVU $(100\,\mathrm{km})^{-1}$. Thick light grey contours: Wind speed climatology at 328K with contours every 10 m s^{-1}, starting at 30 m s^{-1}.

- The region of enhanced PV gradients extends from the US East Coast across the western North Atlantic in a southwest-to-northeast-oriented band (Fig. 10b).

- Over the eastern North Atlantic high PV gradients occure in a broader region, compared to the confined band over the storm track entrance region upstream, indicating higher variability in the position and shape of the tropopause, which is in agreement with higher frequencies of Rossby wave breaking there.

It is noteworthy that at individual time steps, local regions of high PV gradient correlate with the regions of highest wind speed. Consequently, the climatological mean of the PV gradient reaches high values in regions with low variability in the PV gradient and the position of the tropopause. This phenomenon explains the peak in the mean PV gradient over the central United States, where the Rocky Mountains exert a downstream influence that reduces the variability of the troposphere position (Brayshaw et al., 2009).

Figure 11 illustrates the evolution of the North Atlantic jet streaks during the four stages of a jet streak lifetime. At jet streak genesis (Fig. 11c), most centres are located upstream of the Gulf Stream sector and above the continental US. As jet streaks intensify, they generally propagate northeastward (Figure 11a,b). At peak intensification, the variability in jet streak centre positions remains comparatively low and a marked maximum in their occurrence frequency is over the US East coast and the Gulf Stream. Despite the northeastward propagation of jet streaks during their life cycle, the averaged wind speed and PV exhibit minimal change during the four stages of a jet streak life cycle (grey and red contours in Figs 11a–d). This

https://doi.org/10.5194/egusphere-2024-1789
Preprint. Discussion started: 22 July 2024

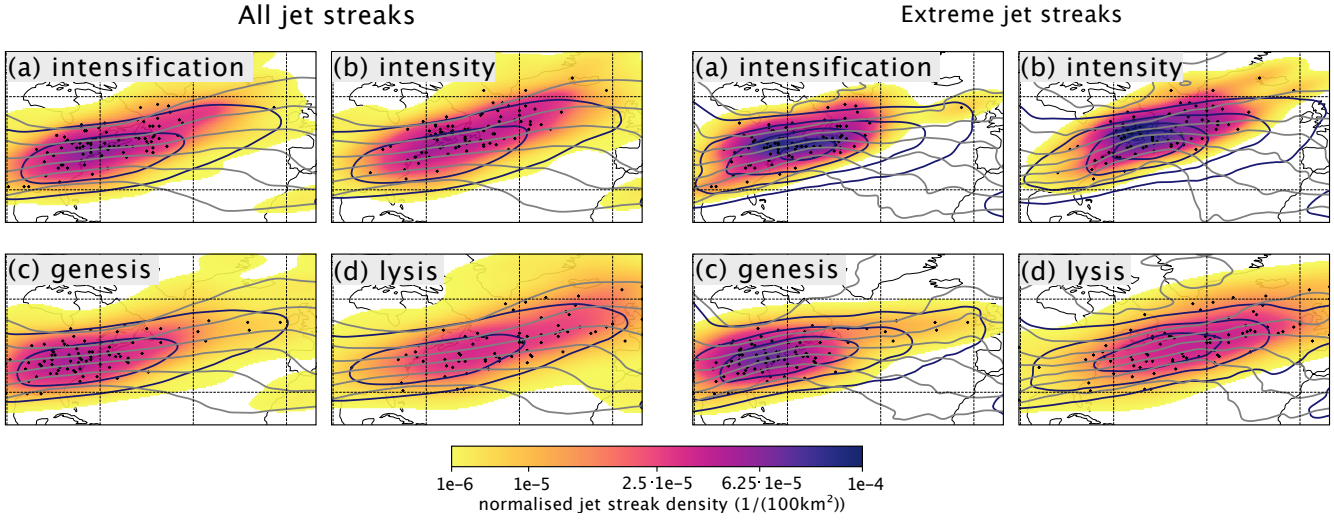

Figure 11. Propagation of (a–d) all and (e–h) extreme North Atlantic jet streaks. Normalised jet streak centre probability density function (PDF) in $(100\,\mathrm{km}^2)^{-1}$ in colours (see Sect. 2.1 for a description of how this is computed). Mean PV field (computed like the mean PV gradient fields in Fig. E1, based on PV fields on the 328 K isentrope for all jet streaks and on the 332 K isentrope for extreme jet streaks) in thick grey contours every 1 PVU starting at 0 PVU, and mean wind speed computed like the PV fields explained above in thick purple contours every $10\,\mathrm{m\,s^{-1}}$ starting at $30\,\mathrm{m\,s^{-1}}$. Black dots represent the centres of extreme jet streaks and are identical in (a–d) and (e–h). For each group of jet streaks, the four panels show the times of genesis – peak intensification – peak intensity – lysis clockwise starting with the bottom left. This order was chose to have the time of peak intensification and intensity in the top row.

370 indicates a significant case-to-case variability in the large-scale dynamic surrounding the jet streak life cycle and motivates a jet streak-centred analysis, which is presented in a following section.

Before we continue with a jet streak-centered analysis, consideration is given to extreme jet streaks and jet stream regimes. Reducing the sample to extreme jet streaks leads to greater consistency between the evolution of jet streak centre positions, the mean PV contours and the mean wind speed (Figs 11e–h). Extreme jet streak centres are more spatially concentrated
375 compared to those of all jet streaks, especially during intensification (Figs 11a–c,e–g). They propagate northeastward and the maximum of the mean wind field increases during the intensification phase (see emergence of third red contour, corresponding to $60\,\mathrm{m\,s^{-1}}$, in Fig. 11e,f) and a small PV ridge at time of peak intensification emerges in the composite (grey contour in Fig. 11e). Nevertheless, the large sample variability complicates the interpretation and necessitates an object-centred analysis.

Finally, the above analysis of the mean large-scale flow during the four stages of jet streak life cycle is repeated with an
380 additional separation into the three jet regimes according to the regime at jet streak genesis Sect. 2.2.1. Figure A1 indeed results in are clearer separation of the large-scale flow, but the case-to-case jet streak variability within each regime remains large. This indicates that the separation into the three jet regimes is not an effective method for reducing case-to-case variability to that

https://doi.org/10.5194/egusphere-2024-1789
Preprint. Discussion started: 22 July 2024

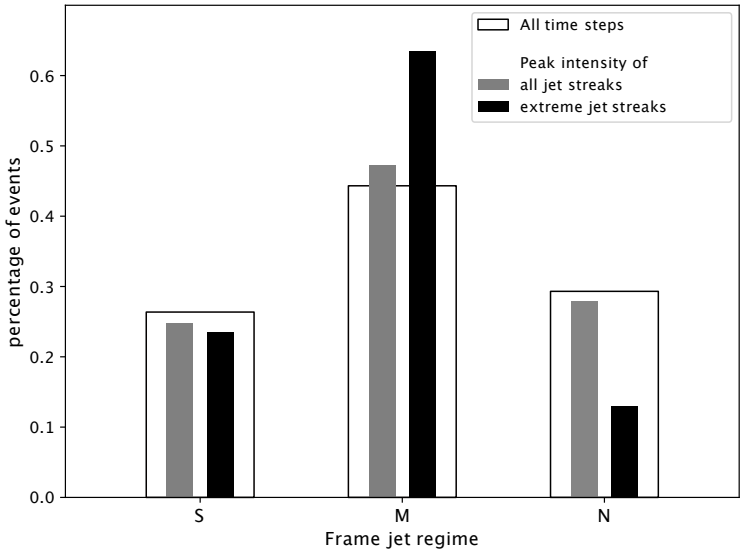

Figure 12. Frequency of times with the low-level jet residing in the S, M, and N regime. Wide white bars: Based on 6-hourly DJF time steps between 1979 and 2023. Light grey bars: As for the white bars, but based on time steps of peak jet streak intensity (in total 1120 time steps). Black bars: As for the wihte bars, but based on time steps of peak jet streak intensity for extreme jet streaks (in total 85 time steps).

point that allows to identify different jet streak life cycles. However, the evolution and occurrence frequency of the different jet regimes during the four stages of a jet streak life cycle warrants further investigation, which is presented in the next section.

3.3 Jet regime occurrence during jet streak life cycles

To explore the link between the jet regimes and the jet streak life cycle, in particular with respect to the intensification of extreme jet streaks, we first analyse the prevalence of the three regimes at the time of peak jet streak intensity. To contextualise the prevalence of each regime, we also evaluate the likelihood of the jet regimes climatologically (white bars in Fig. 12). We also examine the climatological transition probabilities between regimes and compare it to the transition probabilies found during the life cycle of jet streaks.

Based on all jet streaks (grey bars in Fig. 12), we find a slight under-representation of S- and N-regime jet streaks and a slight over-representation of M-regime jet streaks compared to the climatological frequencies. This tendency is accentuated for extreme jet streaks (black bars in Fig. 12), of which 63% peak in the M regime, while the likelihood of N-regime extreme jet streaks is halved compared to all jet streaks.

Figure 13a shows occurrence and transition probabilities between jet regimes at three key moments during the life cycle of a jet streak. Starting with the regime at genesis (28 % in S and N regimes, 47 % in M) there is a larger tendency for the S regime to shift to the M regime and from M to the N regime during the intensification period of a jet streak, which is in agreement with the storm track life cycle argument presented in Ambaum and Novak (2014). At lysis, the relative numbers are fairly similar

https://doi.org/10.5194/egusphere-2024-1789
Preprint. Discussion started: 22 July 2024

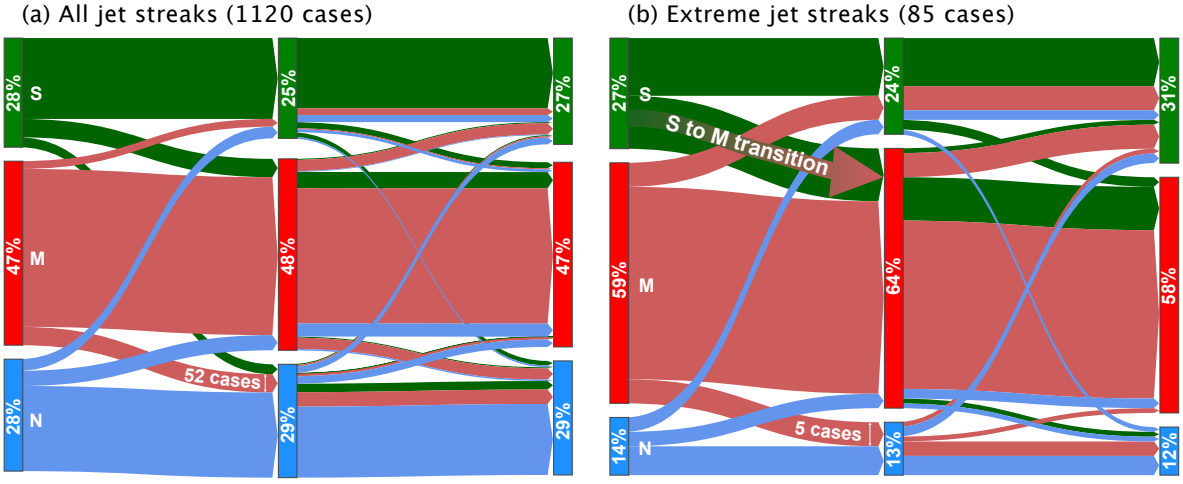

Figure 13. Occurrence of the three jet regimes (green S, red M, and blue N) as jet streaks evolve from genesis (left vertical bar), to maximum intensity (middle bar) and lysis (right vertical bar) for (a) all jet streaks and (b) extreme jet streak. For example, 28 % of all jet streaks are at genesis in the S regime, 47 % in the M and 28 % in the N regime. Arrows indicate the transitions between different jet regimes and the likelihood for a transition is larger for wider arrows, which are scaled according to the number of jet streaks that undergo the corresponding regime transition. For example, from all jet streaks with genesis in the M regime, in 52 cases the jet regime shifts to the S regime at maximum intensity of the jet streak. The colour of each arrow is set by the genesis regime.

to the values at genesis, with M being the most persistent regime. For the extreme jet streaks a notable difference is found (Fig. 13b). The probability of a jet streak originating in the S regime and subsequently transitioning into the M regime during intensification is 48 %. This is more than double the climatological transition probability. Additionally, extreme jet streaks are most likely to occur in the M regime, with the likelihood of extreme jet streaks occurring in a N regime being reduced by a factor of two. During the decay period, there is a greater number of cases where the S regime transitions to the M regime and vice versa, although there is a relatively low number of instances where the N regime is reached. The increased occurrence of the M regime and increased S-to-M transitions during jet streak intensification align with the oscillator model for the North Atlantic storm track life cycle (Ambaum and Novak, 2014). According to this model, baroclinicity is accumulated when the jet is in the S regime, thereby fuelling the potential for strong baroclinic growth. Consequently, baroclinic growth results in an increased eddy momentum transport, thereby intensifying the eddy-driven jet as it transitions into the M regime. The jet is typically strongest in the M regime, which increases the likelihood of the occurrence of extreme jet streaks.

3.4 Jet streak-centred composites

This section explores composites of jet streak-centred wind and PV fields. We start with PV gradient and wind speed at time of peak intensity for non-extreme (Fig. 14a) and extreme jet streaks (Fig. 14b). The PV gradient fields in both displays a Rossby wave with a wavelength of about 6,700 km. The jet streak centre is located at a ridge crest and is anticyclonically curved.

https://doi.org/10.5194/egusphere-2024-1789
Preprint. Discussion started: 22 July 2024

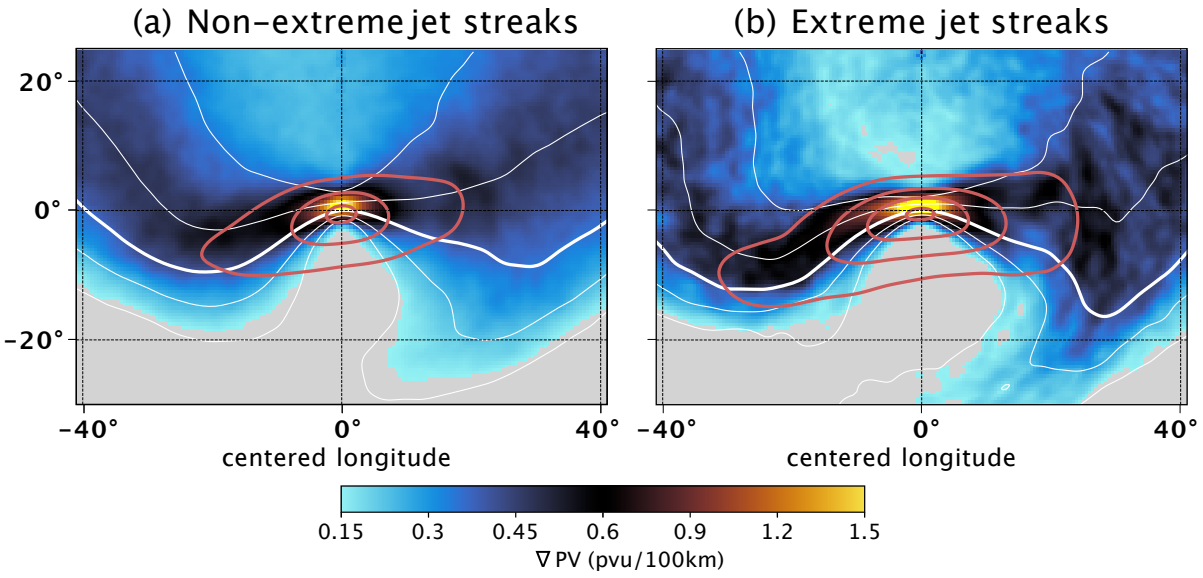

Figure 14. Jet streak-centred composites for (a) non-extreme jet streaks and (b) extreme jet streaks at time of peak intensity. Shown are the (colours) mean of the norm of the PV gradient on central jet streak isentrope, values smaller than 0.15 PVU (100 km)$^{-1}$ are white. Contours show the (white) mean PV for $[0.5, 1.0, 4.0, 6.0]$ PVU on the central isentrope and (bold white contour) 2 PVU, and the (red contours) mean of wind speed on central isentrope, every 20 m s^{-1}, starting at 40 m s^{-1}.

Extreme jet streaks (Fig. 14b) display an advanced stage of PV streamer formation downstream. Maximum wind speeds for extremes is on average 103 m s^{-1} compared to 85 m s^{-1} for non-extreme cases.

The maximum PV gradient is located slightly poleward of the wind speed maximum (Fig. 14a,b), in accordance with the theoretical predictions set forth in Ref. (Bukenberger et al., 2023). The PV gradient maximum is flanked by a minimum on the tropospheric side and a local minimum on the stratospheric side, which is more pronounced in extreme cases. While the standard deviation in the PV gradient composite is relatively small compared with the mean value in the centre (Fig. B1a), both are of a similar order of magnitude up- and downstream of it. This indicates that the intensity of jet streaks is at its maximum when centred on the ridge crest of a Rossby wave. However, the exact positions along the ridge and the shape of the Rossby wave can vary considerably (Fig. B1b). This extensive variability in the composites, which is observed on a case-to-case basis, motivates the implementation of a more detailed clustering approach based on the isentropic PV.

3.4.1 Jet streak-centred SOM clusters

We cluster jet streaks based on jet-streak-centred PV fields at the times of peak intensification and intensity, as detailed in Sect. 2.2. We aim for low similarity between clusters, which imposes an upper limit on the number of clusters and at the same time to keep clusters with clearly different Rossby wave patterns and concentrations of extreme jet streak events separate.

https://doi.org/10.5194/egusphere-2024-1789
Preprint. Discussion started: 22 July 2024

cluster	events	extreme jet streaks	S	M	N	jet isentrope
all	1120	85 (7.5%)	25%	47%	28%	329.4 ± 6.4 K
C0	113	15 (12.0%)	8%	53%	39%	327.6 ± 5.4 K
C1	216	34 (16.0%)	20%	49%	31%	330.6 ± 5.0 K
C2	161	2 (1.2%)	33%	44%	23%	325.0 ± 4.8 K
C3	186	1 (0.5%)	16%	44%	39%	322.1 ± 5.8 K
C4	214	18 (8.8%)	20%	57%	23%	329.6 ± 5.6 K
C5	113	7 (6.5%)	41%	40%	19%	333.0 ± 5.4 K

Table 2. Characteristic properties of the different SOM Clusters. The number of jet streaks as well as extreme jet streaks in each cluster is mentioned and besides the percentage they constitute within the cluster (for example, 12% for cluster 0 containing a total of 113 and 15 extreme events).

Balancing these two goals yields sex clusters, composites of which are shown in Sect. E. The cluster have some interesting commonalities:

1. All clusters show either no or anticyclonic Rossby wave breaking at both the time of peak jet streak intensification and intensity. The tropopause is either straight or anticyclonically curved at the jet streak centre at time of peak jet streak intensity.

2. At time of peak jet streak intensity, all cluster composites show the jet streak centre in the ridge of the Rossby wave, never in a trough.

3. Between the times of peak intensification and intensity, the jet streak centre either remains stationary with respect to the Rossby wave or propagates downstream. Moreover, the amplitude of the composite Rossby wave grows along with the jet streak intensity between the time of peak jet streak intensification and intensity.

Clusters for which this growth is most pronounced (Cluster 0 and Cluster 1, referred to as C0 and C1 in the following) feature the largest fractions of extreme jet streaks: 15 out of 116 anticyclonically oriented jet streaks (12.0%) and 34 out of 216 zonally oriented jet streaks (16%) are extreme cases. Complementary to that, the clusters with the smallest change in Rossby wave amplitude (C2 and C3) have the smallest mean peak jet streak intensity and each contains a fraction of less than 2% of all extreme jet streaks.

Comparing the climatological occurrence frequency of the three jet regimes with their frequency in each cluster shows that strong anticyclonic wave breaking coincides with high frequencies of M and N regimes (for example C0) and more zonal Rossby waves with more frequent S regimes (for example C2 and C5) (Tab. 2).

The clusters differ in the position of the jet streak centre along the Rossby wave ridge and consequently in the orientation of the jet streak. In C0, C3, and C4 (red in Tab. 2), the jet streak centre is positioned upstream of the ridge axis. The jet streaks

https://doi.org/10.5194/egusphere-2024-1789
Preprint. Discussion started: 22 July 2024

in those clusters are oriented SW-to-NE, while the composite Rossby wave shows signs of anticyclonic wave breaking. The stronger the wave breaking of a cluster, the higher is the fraction of extreme jet streaks (e.g., 12% in C0 vs. 0.5% in C3). Two clusters (C1, C2) have the centre of the jet streak positioned at maximum intensity slightly downstream of the ridge axis and the streaks are either zonal (extremes in C1) or have a NW to SE orientation (C2 extremes). Cluster C1, contains the plurality of extreme jet streaks with 34 out of 85 events (16% of the jet streaks in C1 are extreme). Finally, C5 shows a weak Rossby wave with the centre of the straight and zonally oriented jet streak at the Rossby wave crest and with little intensification between the times of peak intensification and intensity.

The large prevalence of SW-to-NE oriented jet streaks and clusters is consistent with Clark et al. (2009), who showed that over the North Atlantic, most jet streaks are southwesterly. Studies of jet streaks in other regions, particularly the eastern North Pacific, show more northwesterly jet streaks, so our clusters are domain- and season-specific to the North Atlantic winter.

We focus in the following on C0 and C1, who both have the largest frequencies of extreme jets and clearly distinct large-scale circulations. Moreover, C0 and C1 are most robust with respect to the SOM clustering parameters. We refer to the former as mostly anticyclonic cases and to the later as zonal cases. For completeness, an analysis of all clusters is shown in Sect. E.

Zonally and anticyclonically oriented jet streak clusters

We start with the Rossby wave patterns in Fig. 15. All anticyclonically oriented jet streaks (C0) intensify upstream of the crest of the Rossby wave, downstream of which we find a pronounced PV streamer. The PV streamer in the extreme jet streak composite grows and bends more anticyclonically between the times of peak jet streak intensification and intensity. This indicates stronger anticyclonic wave breaking for extreme jet streaks (Figure 15a–d). Non-extreme jet streaks tilt southwest-to-northeast at both times, while extreme jet streaks turn to be more zonal as they approach the Rossby wave crest at time of peak intensity (Figure 15c vs. d).

Composites of zonal jet streaks (C1) show a qualitatively different pattern, with a pronounced Rossby wave and zonally oriented composite jet streak at its crest but no PV streamer downstream at time of peak jet streak intensification. A PV streamer develops until the time of peak intensity. Extreme jet streaks feature more pronounced troughs, streamers, and PV cutoffs than non-extreme jet streaks at the time of peak intensity (Figure F1h), and the composite PV streamer grows larger. However, the composite Rossby wave does not bend anticyclonically for either subset of zonally oriented jet streaks. Note that for both clusters, the average increase in maximum wind speed between the times of peak intensification and intensity is similar for non-extreme and extreme jet streaks ($\sim$20 m s^{-1}). The difference in peak intensity stems from already higher intensities of extreme jet streaks at the time of peak intensification.

The maximum of the composite PV gradient as well as the stratosphereward displacement of bands of high PV gradients with respect to the wind speed maximum increase with jet streak intensity for both clusters and all jet streaks (Figure 15a,b vs. c,d and Fig. 15e,f vs. g,h), as expected from theory. The difference in the composite PV gradient between extreme and non-extreme jet streaks is larger at the time of peak intensity than intensification. We hypothesize that the weaker correlation between the wind field and the PV gradient at peak intensification is due to geostrophic imbalance of the rapidly accelerating flow, such that the assumptions required to directly link wind speed to PV gradients (Section 2.5) are violated.

https://doi.org/10.5194/egusphere-2024-1789
Preprint. Discussion started: 22 July 2024

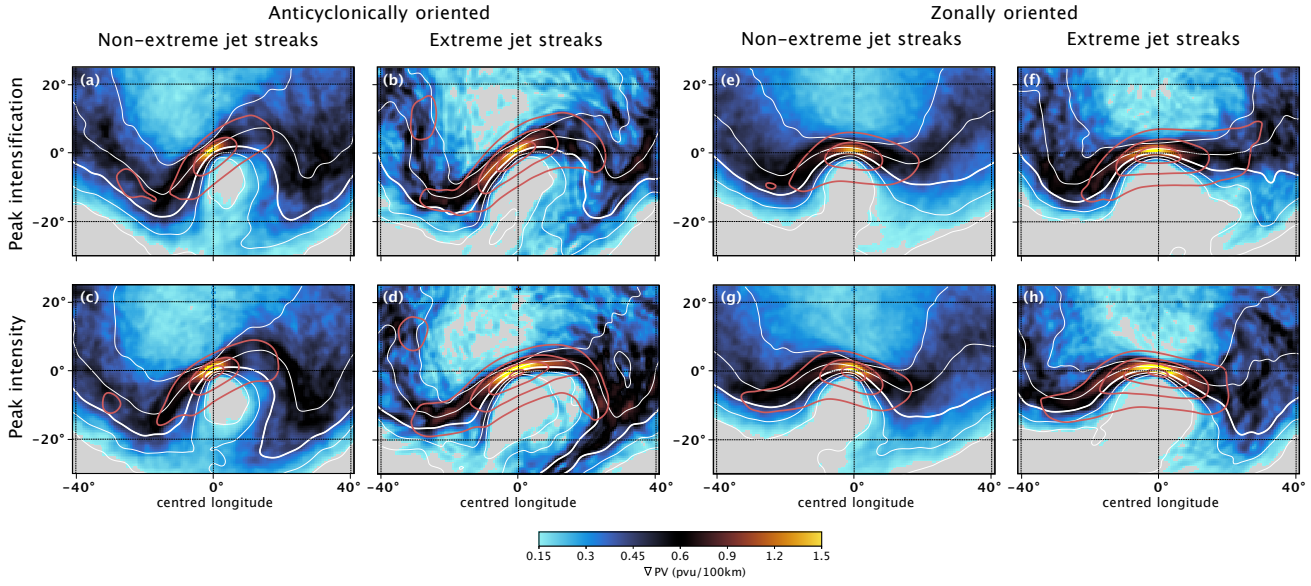

Figure 15. Jet streak centred composites based on (a–d) anticyclonically oriented jet streaks for and (e–h) zonally oriented jet streaks for. Panels (a,b) and (e,f) show composites at the time of peak intensification for (a,e) non-extreme and (b,f) extreme (b,f) jet streaks. Panels (c,d) and (g,h) show the time of peak jet streak intensity for (c,g) non-extreme and (d,h) extreme jet streaks. Colours: PV gradient (PVU (100 km)$^{-1}$), values smaller than 0.15 PVU (100 km)$^{-1}$ are grey. Contours: White: mean PV on central isentrope, thick: 2 PVU; thin: $[0.5, 1.0, 4.0, 6.0]$ PVU; red: wind speed on central isentrope, every 10 m s^{-1}, starting at 40 m s^{-1}.

The PV gradient standard deviation shows more large-scale variability in anticyclonically than zonally oriented jet streaks (Figure F1a–d vs. e–h). Most of the PV gradient variability can be attributed to the variability in the exact shape of the Rossby wave on which the jet streak evolves and the jet streak centre position relative to it. The variability increases as jet streaks reach peak intensity, especially for anticyclonically oriented jet streaks, and especially upstream of the jet streak centre (Figure F1). The standard deviation of PV gradients of extreme jet streaks is larger than that for non-extreme ones far away from the jet streak centre, but notably smaller close to it, for both clusters (e.g., Figure F1a vs. b and Fig. F1c vs. d). This reduced variability indicates that the large PV gradient at extreme jet streak centres is a robust feature.

Finally, consideration is given to lower tropospheric levels for anticyclonically oriented jet streaks (Fig. 16a–d). At time of peak jet streak intensification, we find two surface high-pressure systems on the tropospheric side of the jet: a small anticyclone upstream and an intense one below the right jet exit. The former weakens while the latter intensifies until peak jet streak intensity. An intense and large cyclone is located to the north of the strong anticyclone, below the left jet exit. It exhibits a SLP pattern typical of anticyclonic wave breaking (Thorncroft et al., 1993). This is consistent with the dominance of M- and N-regime jet streaks in the anticyclonic cluster (92%). The composite cyclone is stronger for the non-extreme jet streak (mean SLP of 975 hPa for non-extreme compared to 985 hPa for extreme jet streaks), but the anticyclonic is notably stronger for the extreme cases (1035 hPa vs. 1015 hPa), which results in a meridional pressure gradient that is about 25 % for the extreme cases

https://doi.org/10.5194/egusphere-2024-1789
Preprint. Discussion started: 22 July 2024

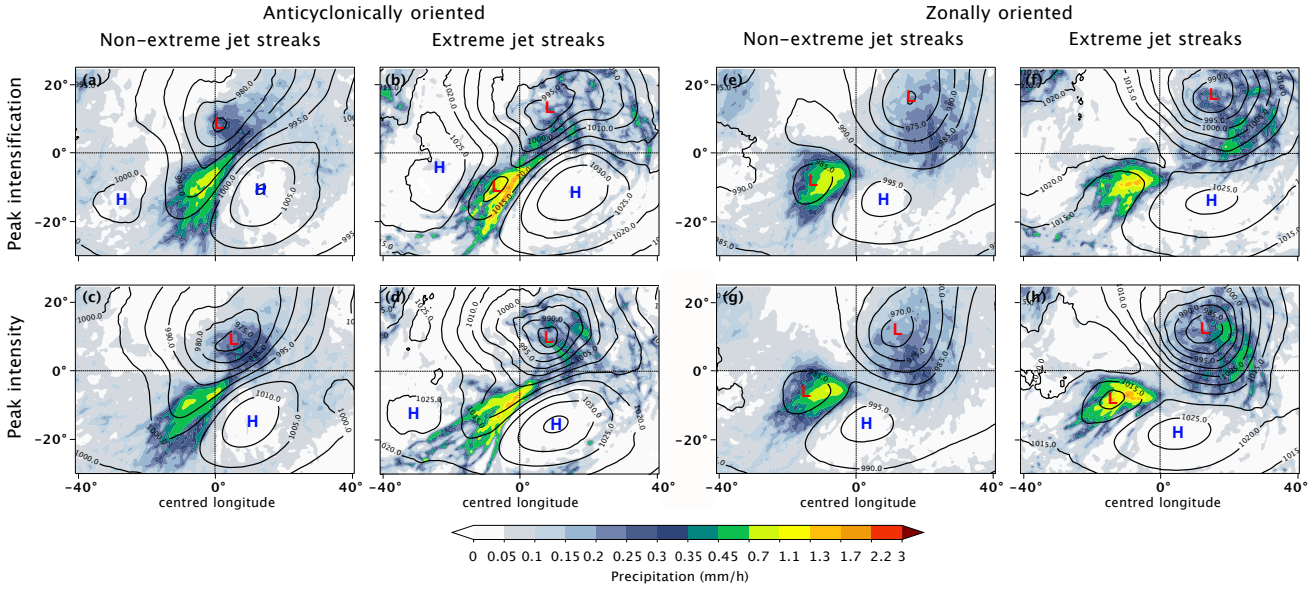

Figure 16. Jet streak-centred composites for (first two columns) anticyclonically oriented jet streaks and (last two columns) zonally oriented jet streaks. Top row for time of peak intensification and bottom row for peak intensity. Each panel is sub-divided into non-extreme (first and third column) and extreme (second and fourth column) jet streaks. Shading: hourly precipitation (mm h^{-1}). Contours: mean sea level pressure, every 5 hPa starting at 970 hPa.

. The cyclone is associated with an elongated SW-to-NE oriented band of enhanced precipitation along its cold front and the maximum in cold-frontal precipitation is located below the right jet entrance. Precipitation there is more intense for extreme jet streaks.

Precipitation intensity changes only marginally between the times of peak intensification and intensity (Fig. 16a – d). However, the precipitation rate is markedly larger for extreme than non-extreme jet streaks, in particular below the right jet streak entrance (compare the first vs. second column in Fig. 16).

To relate these results to previous literature on cross-isentropic mass flux in warm conveyor belts (WCB), WCB frequencies at 400 hPa (Fig. 17a–d) complement the analysis of low-level dynamics. They show little change during the lifetime of non-extreme anticyclonically oriented jet streaks. Most WCB outflow occurs on the tropospheric side of the jet axis. The left jet exit, which exhibits slightly stronger precipitation, also shows more WCB outflow for extreme jet streaks. Consistent with the precipitation patterns, WCB outflow feeding into the Rossby wave ridge is more frequent for extreme than non-extreme jet streaks (Figure 17a,c vs. b,d) and exceeds 80% in grid points close to the Rossby wave crest as extreme jet streaks reach peak intensity.

In the cluster of zonally oriented jet streaks (C1) only a single surface anticyclone exists, which does not intensify between peak jet streak intensification and intensity. However, it approaches the jet streak centre from the right jet exit on the tropospheric side (Figure 15e–g). A mature cyclone resides below the left jet exit and the cyclone-anticyclone pear appears more

https://doi.org/10.5194/egusphere-2024-1789
Preprint. Discussion started: 22 July 2024

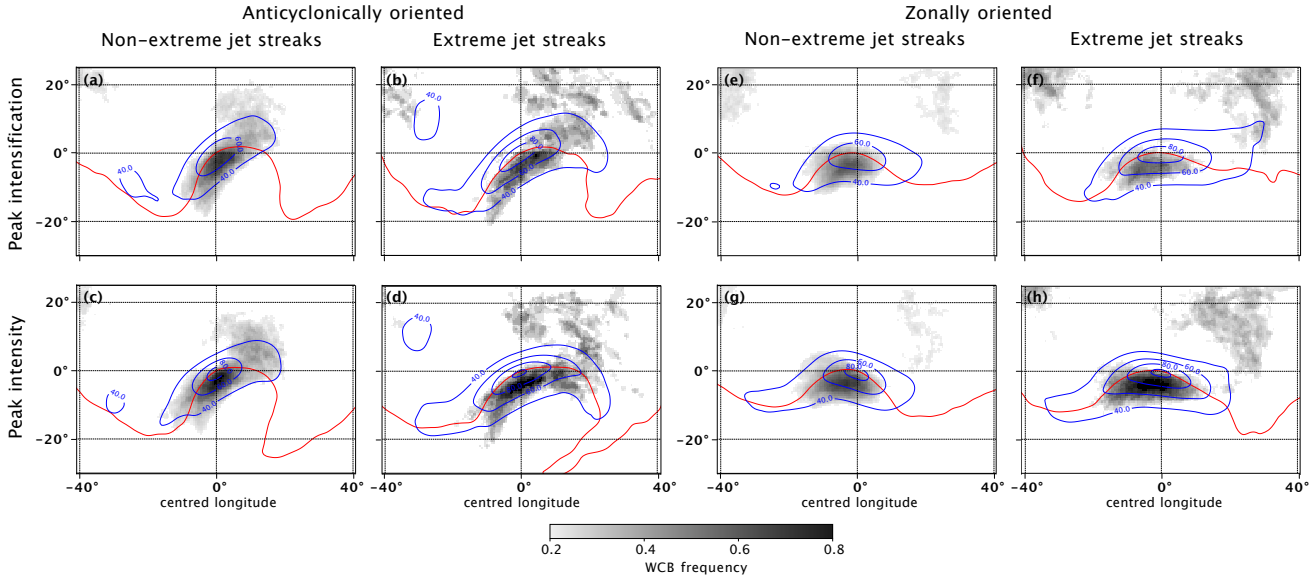

Figure 17. Jet streak-centred composites for (first two columns) anticyclonically oriented jet streaks and (last two columns) zonally oriented jet streaks. Top row for time of peak intensification and bottom row for peak intensity. Each panel is sub-divided into non-extreme (first and third column) and extreme (second and fourth column) jet streaks. Colours: WCB outflow frequency on 500 hPa. Contours: red: mean PV on central isentrope, 2 PVU, blue: mean of wind speed on central isentrope, every 20 m s^{-1}, starting at 40 m s^{-1}.

meridionally aligned for extreme cases. In the warm sector of the mature cyclone, the precipitation rate for extreme jet streaks is approximately double that of non-extremes. The pressure difference between the cyclone-anticyclone pair is roughly 45 hPa during peak jet streak intensity compared to 30 hPa for non-extreme cases. As is the case for anticyclonically oriented jet streaks, the difference in the meridional pressure gradient between extreme and non-extreme jet streaks primarily stems from the intensity of the anticyclone.

The most remarkable difference in the synoptic situation between the clusters of zonally and anticyclonically oriented jet streaks is the presence of a second, mesoscale surface low upstream below the right jet entrance of zonally oriented jet streaks. It grows and produces more precipitation as jet streaks reach peak intensity, again with more precipitation in extreme jet streak composites. For anticyclonic cases, no upstream cyclone but rather an upstream anticyclone is found.

Similar to the anticyclonic cluster, WCB outflow on the tropospheric side of the jet is more frequent for extreme zonally oriented jet streaks (Fig. 17a–d vs. e–h). Notably, WCB frequencies in this region almost doubles between the times of peak intensification and intensity for extreme jet streaks, but barely changes for non-extreme jet streaks (Fig. 17e–h). WCB outflow in the left jet exit is very rare for non-extreme zonally oriented jet streaks, but more frequent for extreme cases. The WCB frequencies indicate enhanced cross-isentropic mass flux as expected also from more intense precipitation rates.

https://doi.org/10.5194/egusphere-2024-1789
Preprint. Discussion started: 22 July 2024

4 Conclusion and Outlook

This study analyzes the evolution of North Atlantic winter (DJF) jet streaks from January 1979 to February 2023, using 6-hourly ERA5 data. The analysis is based on an object-centred identification and tracking framework, identifying jet streaks based on the isentrope of maximum wind speed. The proposed method ensures robust identification of jet streaks, independent of their varying heights. We first investigate basic characteristics of North Atlantic winter jet streaks and later combine the results with object-centred composites to study jet streak life cycles in various flow situations. To investigate the connection between jet streaks and the eddy-driven jet stream, the results are categorized based on jet stream regimes defined by Frame et al. (2011). Furthermore, the study groups jet streaks into different clusters based on isentropic PV using a self-organising map algorithm in an attempt to establish a link between jet streaks and different phases of Rossby wave development. To the best of our knowledge, this is the first systematic comparison of extreme and non-extreme jet streaks and the results indicate that extreme jet streaks can develop in association with different weather systems but are always developing under an increased influence of diabatic processes. The following sections discuss the most important findings of this study in more detail, point out key limitations, and lay out a possible avenue for future research.

4.1 Characteristic properties of extreme North Atlantic winter jet streaks

The peak intensity of North Atlantic wintertime jet streaks is $87\pm9\,\mathrm{m\,s^{-1}}$ ($104\pm9\,\mathrm{m\,s^{-1}}$ for extreme jet streaks). The maximum wind speed reached during a jet streak life cycle correlates with the maximum PV gradient and the lifetime of events, which is is 1.4 times longer for extreme than for all jet streaks. However, the intensification rates, measured in change in wind speed per 6-hourly time step, are similar for extreme and non-extreme jet streaks. This result indicates that extreme jet streaks are distinguished by a prolonged strengthening period rather than increased intensification rates.

Jet streaks propagate across the North Atlantic from southwest to northeast throughout their life cycle and extreme jet streaks tend to propagate larger distances during their intensification, which is in agreement with their prolonged intensification period. Categorising jet streaks based on the Frame jet regimes at time of peak jet streak intensity shows that the frequency of the three jet regimes, which are intricately linked to the state of the North Atlantic storm track (Frame et al., 2011; Woollings et al., 2010), are equally distributed at peak jet streak intensity as they are climatologically. This finding suggests that a finer-grained clustering of jet streaks is needed to understand their variability from case to case. A notable exception is the increased occurrence frequency of the zonal jet regimes (M regimes) during times of extreme jet streaks. Also, the transition from an equatorward to a zonal jet regime (S to M) occurs with increased probability during extreme jet streaks. This suggests that the enhanced baroclinicity normally observed during S regimes leads to strong baroclinic development, which might be conducive to the sustained intensification period characteristic for extreme jet streaks.

4.2 Large-scale flow situation during jet streak evolution

A self-organising map (SOM) algorithm clustering of upper-level PV at the time of maximum jet streak intensity results in six clusters, which display the following main characteristics:

https://doi.org/10.5194/egusphere-2024-1789
Preprint. Discussion started: 22 July 2024

1. At time of peak jet streak intensity, the jet streak centre is always located close to the axis of a Rossby wave ridge. In anticyclonic Rossby waves, the jet streak is located slightly upstream of the ridge axis during peak intensification and at peak intensity. In zonally oriented Rossby waves the jet streak is located at the ridge axis.

2. No cluster mean exhibits well-marked cyclonic Rossby wave breaking at the times of peak intensification or at the time of peak intensity.

The two clusters that contain the majority of extreme jet streaks are investigated in more detail with a focus on the time of maximum jet streak intensity. The first cluster is zonally oriented and contains a total of 216 (34 extreme) events. The second cluster is anticyclonically oriented, with 15 extreme jet streaks out of 113 total events. For zonally oriented jet streaks, we find a mature Rossby wave in upper-level PV composites that intensifies along with the jet streak. The jet streak centre is collocated with the axis of the Rossby wave ridge at time of peak jet streak intensity. At the surface, near the left jet streak exit, a mature extratropical cyclone is identified. It is accompanied by warm-sector precipitation, which is more intense for extreme than non-extreme jet streaks. Beneath the right jet streak entrance, a small but intensifying mesoscale cyclone produces intense precipitation. The warm conveyor belt outflow that is associated with this smaller low-pressure system feeds the upper-level ridge. Anticyclonically curved jet streaks form on a Rossby wave with strong anticyclonic wave breaking. The jet streak centre is located upstream of the ridge axis at peak intensity. In contrast to the two cyclones in the right entrance and left exit of zonally oriented jet streaks, only the mature cyclone centred poleward of the left jet exit is present in the low-level composites for anticyclonically oriented jet streaks. The precipitation below the right jet streak entrance is associated with the elongated upstream extension of the cold front attending the mature extratropical cyclone in the left exit. The two clusters have different upper-level Rossby wave patterns and lower-level weather systems, but share key characteristics, particularly in the differences between extreme and non-extreme jet streaks. Composites based on extreme events show larger Rossby wave amplitudes and higher warm conveyor belt frequencies for both clusters. The low-level circulation is characterised by an anticyclone southwest of the jet streak centre and a strong cyclone below the left jet exit. Precipitation is more intense in extreme cases, as expected from the increased cross-isentropic motion in the rising warm conveyor belt. The composites also indicate the important role of an anticyclone located below the right jet streak exit. The difference in the meridional pressure gradient in the jet streak exit region between extreme and non-extreme cases is primarily due to a stronger anticyclone rather than a deeper cyclone.

4.3 Outlook

Diabatic processes play an increased role in extreme jet streaks, a result that has important implications for numerical modelling and predictability of these events. A warmer and therefore more humid atmosphere has more potential for diabatic heating of clouds. Understanding the role of diabatic PV modification in the evolution of jet streaks is therefore also important for shaping our expectations of trends in the frequency and intensity of extreme jet streak events in a warming climate. Our next step is therefore to perform a detailed quantitative analysis of the influence of diabatic processes on jet streak intensification and, in particular, on extreme jet streaks. Such an analysis is the focus of the next part of this study, which uses the Lagrangian PV gradient framework for jet streak evolution. The framework has proven useful in quantifying the role of diabatic processes

https://doi.org/10.5194/egusphere-2024-1789
Preprint. Discussion started: 22 July 2024

on jet streak dynamics in case studies (Bukenberger et al., 2023), and combining it with jet streak-centred composites over a reanalysis data period will improve the mechanistic understanding of diabatic-adiabatic coupling in jet streak dynamics.

4.4 Limitations

The jet streak tracking algorithm has two key limitations. First, its restricted domain, and second the fact that it detects only one jet streak centre at a time.

The confinement to the North Atlantic domain leads to inaccuracies in capturing the genesis and lysis of jet streaks as they reach the domain boundary. We estimated the effect of this limitation by identifying jet streaks with genesis or lysis near the boundaries of the North Atlantic domain and compared their lifetimes to jet streak that reside well within the domain throughout their evolution (Figure C1). The results indicate that primarily strong and long-lived jet streaks are affected by the domain boundaries, such that this limitation mainly affects the the longest life cycles. Moreover, jet streaks that start (end) by entering (leaving) the domain typically reach their strongest intensification and intensity well within the domain, such that this limitation does not affect those key lifecycle stages.

Detecting only one jet streak at a time runs the risk of missing weak jet streaks while stronger ones are present, potentially biasing weak jet streaks towards shorter durations or missing them altogether. We compared the lifetimes of jet streaks whose genesis or lysis happens directly after the lysis or before the genesis of another jet streak in the domain to the lifetimes of jet streaks for which this is not the case. Since both groups have similar lifetime distributions and mean intensities (Figure C1), the link between jet streak intensity and duration is unlikely to be caused by this method limitation.

We believe that for the focus of this study – peak jet streak intensification and intensity – neither the domain boundaries nor the inability to track multiple concurrent jet streaks, will meaningfully impact our findings. A more flexible algorithm allowing for multiple concurrent jet streaks is currently under development and will be used in follow-up studies.

https://doi.org/10.5194/egusphere-2024-1789
Preprint. Discussion started: 22 July 2024

Appendix A: Jet streak paths over the North Atlantic

To understand the extent to which the variability in jet streak paths can be explained by the eddy-driven jet, we compiled normalized jet streak centre PDFs over the North Atlantic for S-, M- and N-regime jet streaks. Figure A1 shows that jet streaks in all regimes tend to evolve from southwest to northeast. Figure A1a–d illustrates the paths of S-regime jet streaks, which are predominantly zonal. Notably, and consistent with their longer lifetimes (Section 3.1), extreme jet streaks in this category tend to propagate farther eastward compared to average S-regime jet streaks (Figs A1b–d). The composite wind speed and PV fields remain qualitatively unaltered throughout S-regime jet streak evolution.

M-regime jet streaks propagate northeastward, and most of them reach peak intensity at their northernmost position. The composite jet stream intensifies along with them and tilts northeastward throughout their entire evolution. The concurrent intensification of the composite jet stream and M-regime jet streaks is due to a large concentration of jet streak centres in the meridional direction, especially at times of peak intensification and intensity (Fig. A1e–h). The PV composite indicates Rossby wave intensification along with jet streak intensification (grey contours in Fig. A1f,g). N-regime jet streaks are either near-stationary close to the North American East Coast or propagate northeastward across the North Atlantic. Some N-regime jet streaks turn southward between the time of peak intensity and lysis, with the PV field indicating anticyclonic wave breaking (Figure A1i–l). While we find different mean jet streak centre paths for each Frame regime, the variability in jet streak paths for each remains similarly large as that of all jet streaks. While the normalized PDFs show some signatures of the different jet regimes, the PDFs of all groups is broad, implying that the bulk of variability in jet streak evolution over the North Atlantic cannot be explained by the state of the eddy-driven jet.

Another way to investigate the coupling between lower and upper levels is to compare the mean state of the upper-level jet during peak jet streak intensity in different Frame jet regimes with the lower-level composites.

Figure A2 shows differences in Rossby wave patterns between upper (328 K) and mid (310 K) levels for S- and N-regime jet streaks. For S-regime jet streaks, the composite jet at upper levels exhibits a westward compared to that at lower levels. The composite at lower levels shows cyclonic Rossby wave breaking but that at upper levels does not. For N-regime jet streaks, the Rossby wave pattern at upper levels is less clear compared to the anticyclonic wave breaking at lower levels, probably due to greater variability at upper levels (Figure A2j vs. l). M-regime jet streaks show consistent Rossby wave patterns at upper and lower levels, suggesting enhanced vertical coupling. This result points toward an increased interaction between upper and lower levels for jet streaks that peak in the M regime and is consistent with the finding that most extreme jet streaks peak in the M regime and show enhanced lower-level-to-upper-level coupling.

https://doi.org/10.5194/egusphere-2024-1789
Preprint. Discussion started: 22 July 2024

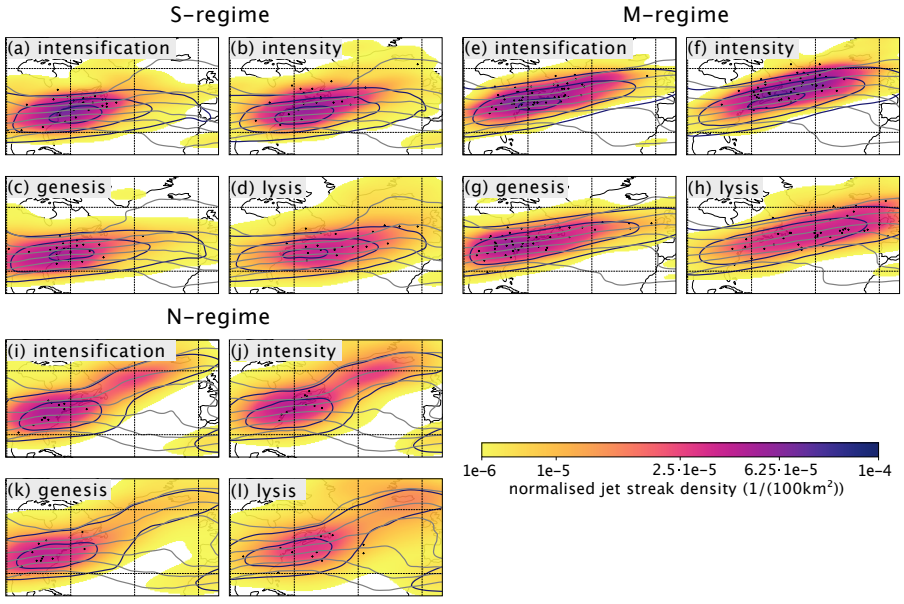

Figure A1. Life cycles of all jet streaks grouped by Frame regime. Like Fig. 11 (a – d), but now for S- (a – d), M- (e – h), and N-regime (i – l) jet streaks.

Appendix B: Standard deviation of PV gradients

Figure B1 shows the jet streak centred standard deviation of PV gradients and wind speed for (Figure B1a) non-extreme and (Figure B1b) extreme jet streaks. It illustrates the variability of the dynamical environment in which jet streaks develop, but also the utility of the centred composites, as the standard deviation of the PV gradient is low close to the composite jet streak centre. Extreme jet streaks seem to evolve in two clusters, as can be seen by the two regions of enhanced variability in wind speed southwest and northeast of the composite extreme jet streak centres (Figure B1b). The overall large variability in the large-scale dynamical environment around jet streak centres at peak jet streak intensity motivates the clustering of jet streaks into different dynamical regimes.

https://doi.org/10.5194/egusphere-2024-1789
Preprint. Discussion started: 22 July 2024

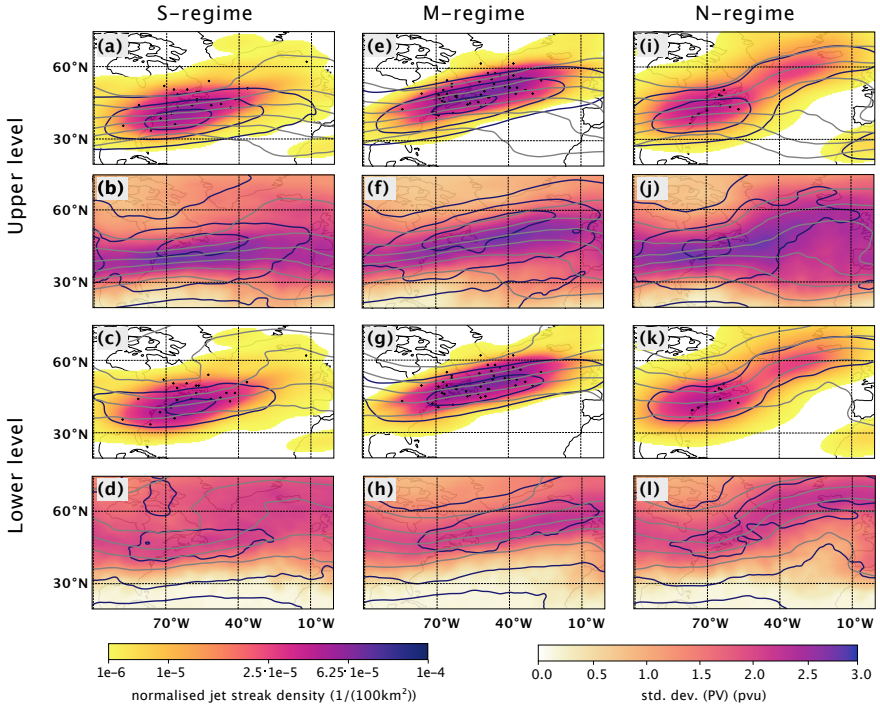

Figure A2. Characteristics of large-scale flow at peak jet streak intensity on the (rows 1–2) central isentrope and at (rows 3–4) 310 K, for jet streaks in the (first column) S, (second column) M and (third column) N regime. First row like (b,f,j) in Fig. A1 and third row like (b,f,j) in Fig. A1, but with PV and wind speed at 310 K instead of on the central jet streak isentrope. The second row shows (in colours the standard deviation of PV on central jet streak isentropes at time of peak jet streak intensity, the (black contours) standard deviation of wind speed on central jet streak isentropes at time of peak jet streak intensity, starting at 10m s^{-1}, at intervals of 10m s^{-1}. Grey contours: Like grey contours in (i). The forth row shows the same variables as the second row, but with all variables on 310 K instead of the central jet streak isentrope.

Appendix C: Lifetimes for jet streaks with different characteristics

To test whether the limitations of the jet streak tracking algorithm of tracking only one object at a time and being limited to the North Atlantic domain cause biases that call into question the reliability of our results, especially concerning the correlation between peak intensity and lifetime of jet streaks, we extracted jet streaks with different characteristics that should be affected by those two limitations. Figure C1 shows that, first, jet streaks whose lifetime is limited by the North Atlantic domain boundary tend to have longer lifetimes than those that stay within the domain throughout their entire evolution (compare dark blue and dark red boxes). The distribution of their peak intensities is also shifted to higher values (not shown). This indicates that, if anything, this limitation leads to an under-estimation of the correlation between peak jet streak intensities and lifetimes.

Jet streaks with genesis/lysis directly after/before the lysis/genesis of another jet streak tend to live longer than those that emerge without another jet streak beginning/ceasing to exist. However, the difference is marginal compared to the variability

https://doi.org/10.5194/egusphere-2024-1789
Preprint. Discussion started: 22 July 2024

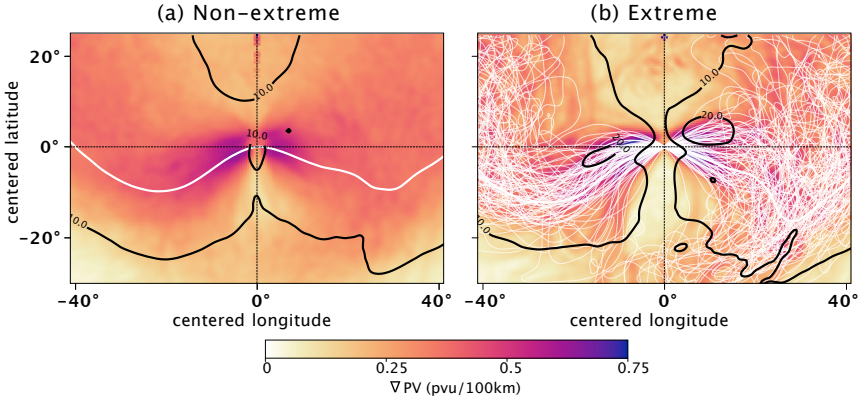

Figure B1. As for Fig. 14, but with the standard deviation of PV gradient instead of PV. Contours: White: PV on central isentrope, 2 PVU, black: standard deviation of wind speed on central isentrope, every 10 m s^{-1}, starting at 10 m s^{-1}, white dashed in (b): 2 PVU isolines for all central isentropes of extreme jet streaks at peak jet streak intensity.

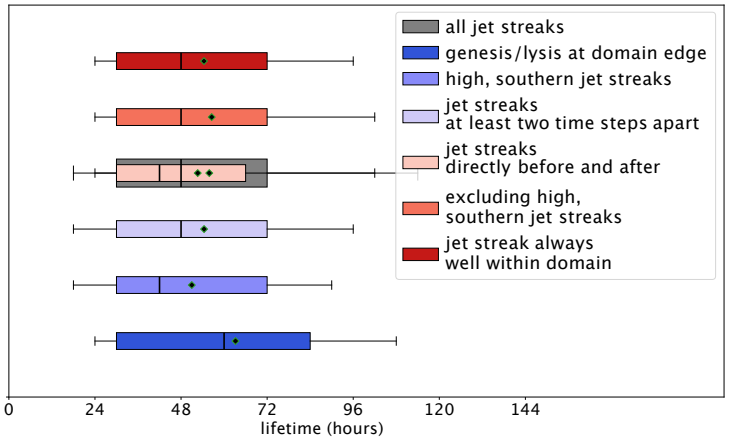

Figure C1. As for Fig. 9, but now for jet streaks with different characteristics. genesis/lysis at domain edge: those that begin or end by entering/leaving the North Atlantic domain; jet streaks always well within domain: all jet streaks except for those that begin or end by entering/leaving the North Atlantic domain; jet streaks at least two time steps apart: jet streaks that begin and end at least two time steps after/before the jet streak preceding/following them ceases/begins to exist; jet streaks directly before and after: jet streaks that begin directly (i.e., one time step) after the jet streak preceding them has ceased to exist and end directly before the next jet streak is generated; high, southern jet streaks: the jet streak centre remains south of 30°N and warmer than 334 K throughout its evolution.

of the entire dataset. From these two results, we conclude that while the limitations of the jet streak tracking algorithm cause an overall bias toward shorter lifetimes, the correlation between peak jet streak intensity and lifetime is robust.

https://doi.org/10.5194/egusphere-2024-1789
Preprint. Discussion started: 22 July 2024

Appendix D: Description of SOM Clustering Method

In this study, we use an unsupervised Self-Organizing-Map algorithm and subsequent hierarchical agglomerative clustering of the SOM output. The process is described in the following sections.

D1 Data Processing

Our input data consists of 1120 2d-PV-fields for two timesteps – maximum intensification and maximum wind intensity of the respective jet streak events. To pass this data to the algorithm, we first reshape the PV-fields for both timesteps into a 2d-array, in which axis 0 represents the 1120 events and axis 1 contains PV values for each grid point. Then we merge these two arrays along axis 1. Additionally, the PV values are normalized to values between 0 and 1 using the following the description of minimum-maximum-scaling by Pedregosa et al. (2011):

$$\mathrm{PV}_{\mathrm{scaled}} = \mathrm{PV}_{\mathrm{std}} \cdot (\max - \min) + \min = \mathrm{PV}_{\mathrm{std}} \cdot (1 - 0) + 0, \tag{D1}$$

where

$$\mathrm{PV}_{\mathrm{std}} = \frac{\mathrm{PV} - \mathrm{PV}_{\min}}{\mathrm{PV}_{\max} - \mathrm{PV}_{\min}} \tag{D2}$$

and 'max $(= 1)$' and 'min$(= 0)$' represent the value range of the scaling.

D2 Self-Organizing-Map Algorithm

As described in Sect. 2.2, the SOM algorithm produces a map of nodes whose reference vectors represent the input data space. We follow the method described by Hewitson and Crane (2002):

1. Define the number of nodes via the mapsize $(m \times n)$.
2. Start initialization of the reference vectors (sometimes also referred to as 'weights') using eigenvectors and eigenvalues produced through Principal Components Analysis (PCA). This approach minimizes computational effort (Kohonen, 1995). The resulting reference vectors have the same dimensions as our input data vectors.
3. We now present each of our 1120 input data vectors to the SOM. The algorithm compares all reference vectors with the input data vector, computes the Euclidean distance between them and chooses the reference vector with the smallest Euclidean distance as the 'best-matching-unit (BMU)'. Now, each input vector is assigned one reference vector as its BMU. Using this information, we can adjust the reference vectors to bring them closer to their associated input vectors. Following the approach by (Vesanto et al., 2000) we first compute the sum of all input vectors per BMU:

$$\mathbf{s}_j(t) = \sum_{k=1}^{n_{V_j}} \mathbf{x}_k \tag{D3}$$

https://doi.org/10.5194/egusphere-2024-1789
Preprint. Discussion started: 22 July 2024

where $\mathbf{x}_k$ are all the input vectors per node j and n_{V_j} the number of input vectors per node j. After that we update all nodes:

$$\mathbf{m}_i(t+1) = \frac{\sum_{j=1}^{a} h_{ij}(t)\mathbf{s}_j(t)}{\sum_{j=1}^{a} n_{V_j}(t)h_{ij}(t)} \tag{D4}$$

where $\mathbf{m}_i$ is the reference vector of the node i to be updated ($i = 1, 2, ..., 35$), a is the total number of nodes, h_{ij} is the neighbourhood function or smoothing kernel, $\mathbf{s}_j$ is the sum of all input vectors per node j and n_{V_j} the number of input vectors per node j. In our case, the neighbourhood function is a Gaussian function:

$$h_{ij} = \exp(-\frac{\|\mathbf{r}_\mathrm{i} - \mathbf{r}_j\|^2}{2\sigma^2(t)}), \tag{D5}$$

where $\mathbf{r}_\mathrm{i}$ and $\mathbf{r}_j$ are the location vectors of node i and node j in the map space and σ defines the width of the kernel. With increasing $\|\mathbf{r}_\mathrm{j} - \mathbf{r}_i\|$, h_{ij} converges towards 0, such that nodes far away from node i contribute only marginally to its updating.

4. This procedure loops through several iterations, during each of which the kernel width σ is monotonically reduced. The loop stops as soon as the reference vectors do not change anymore. Each of the resulting nodes contains a normalized PV vector approximating the mean of the associated input vectors.

To find an optimal mapsize $m \times n$, we assess the quantization and the topographic error for different mapsizes. The quantization error is the average euclidean distance of input vectors to their respective BMUs and thus the smaller the value the more homogeneous the clusters (Kohonen, 1995). Additionally, we can examine the topographic error, which tells us how well the SOM preserves the topology of the input data. It is the ratio of the events whose first and second BMUs are not neighbours on the map to the number of all events. The smaller the value, the more similar adjacent nodes(Kiviluoto, 1996). We compare different map sizes in terms of their quantization and topographic errors and the number of empty nodes produced. Empty nodes do not have an associated input data vector and are understood as a sign of a map that is too large. A suitable map size with a low topographic error and no empty nodes turns out to be a 7×5 map.

D3 Hierarchical Agglomerative Clustering

After using the SOM algorithm to reduce the dimensionality of our data set, we performed hierarchical agglomerative clustering on the resulting reference vectors, using Ward-Linkage (Ward, 1963). This clustering works as follows:

1. Merge two nodes into a cluster according to the Ward criterion, i.e. such that the sum of the squared deviations about the group mean is minimized.

2. Compare all newly formed clusters and use the Ward criterion to decide which clusters to merge into a larger cluster. In this way, all possible cluster combinations are compared. The pairs with the smallest increase in the sum of the squared deviations from the group mean are finally merged.

https://doi.org/10.5194/egusphere-2024-1789
Preprint. Discussion started: 22 July 2024

3. Pairs of clusters are successively merged until all clusters have been merged into one big cluster. The result can be visualized as a dendrogram.

4. Decision upon number of clusters is based on the dendrogram output. We set the maximum allowed cophenetic distance (describes the height of the dendrogram where two branches are joined together) to 25, which results in 6 clusters.

Appendix E: Jet streak evolution over the North Atlantic

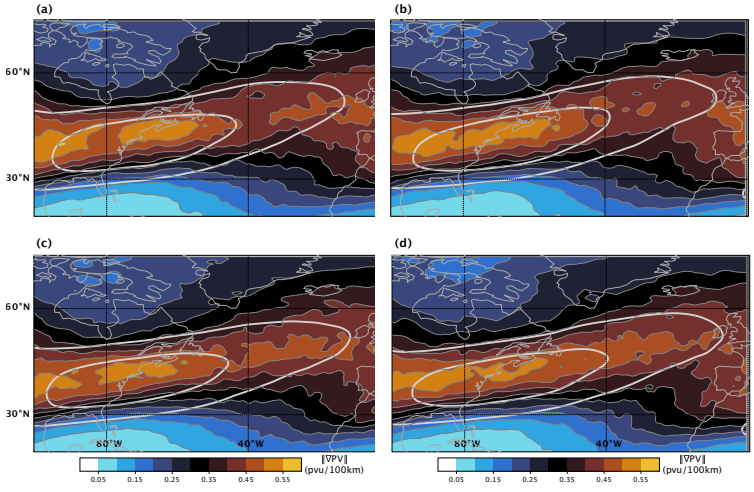

Figure E1. As for Fig. 10(b), but now only for characteristic time steps of jet streak evolution. (a): Climatology across all time steps of maximal jet streak intensification. PV gradient and wind speed fields on the central isentrope of the jet streak at time of strongest intensity for each individual jet streak are considered and the resulting 1120 PV gradient and wind speed fields are averaged to gain the climatology. (a, c, d): As for (b), but now for the time of strongest intensity, start and end of jet streak evolution, respectively. Note that we consider PV and wind speed fields on the central isentrope of the jet streak at time of strongest intensity for all 4 climatologies.

Appendix F: Composite analysis of jet streak clusters

To assess how robust our results are, we present the standard deviation of jet streak centred PV gradients for jet streaks in C0 and C1 (Figure F1). We find that while both clusters show substantial variability for extreme as well as non-extreme cases, the large-scale structure of the Rossby waves on which jet streaks reach their peak intensity is robust (anticyclonic RWB for C0 and a Rossby wave with the jet streak downstream of the ridge axis in C1).

Figure F2 shows the composites for low-level weather systems for all cluster to be similar for clusters with similar upper-level RW patterns (Compare Fig. F2A,D,E and Fig. F4A,D,E as well as Fig. F2B,C,F and Fig. F4B,C,F). Figure F3 illustrates

https://doi.org/10.5194/egusphere-2024-1789
Preprint. Discussion started: 22 July 2024

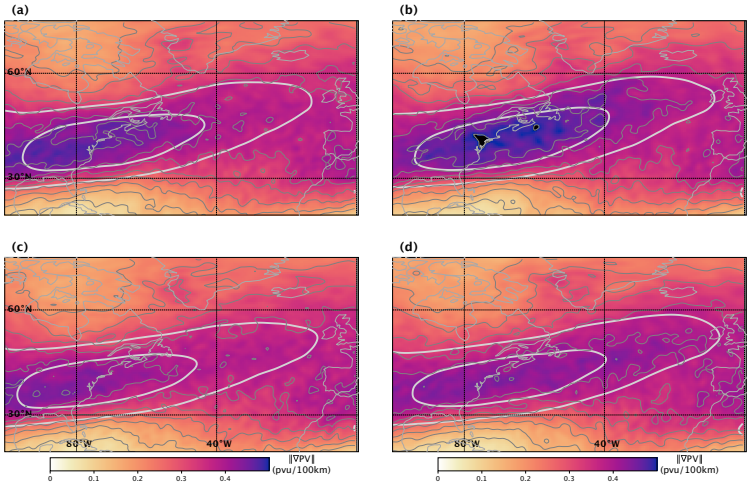

Figure E2. As for Fig. E1, but now with the standard deviation of PV gradients across all jet streaks in colour and thin grey contours every 0.05 PVU (100 km)$^{-1}$.

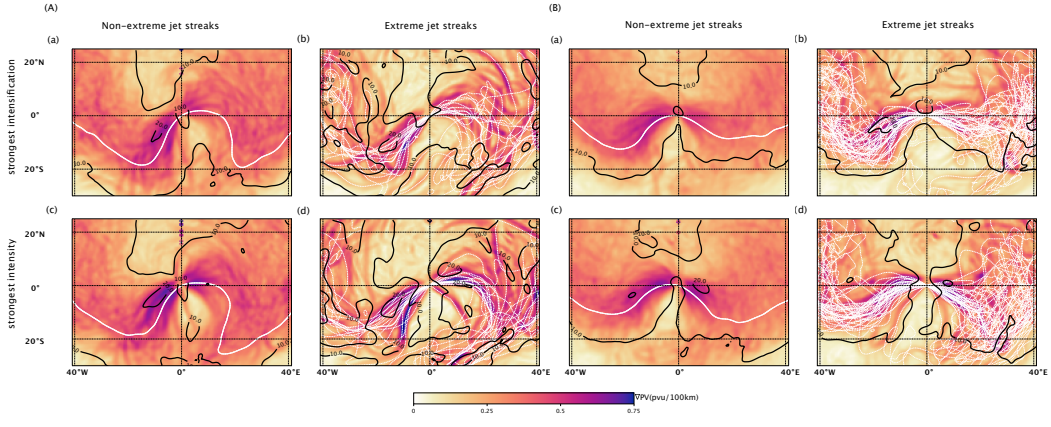

Figure F1. jet streak centred composites based only on jet streaks in C0 for (a–d) and C1 for (g–h). Panels (a, b) and (e, f) show composites at the time of peak intensification for non-extreme (a,e) and extreme (b,f) jet streaks. Panels (c, d) and (g, h) show the time of peak jet streak intensity for non-extreme (c, g) and extreme (d, h) jet streaks. Colours: standard deviation of PV gradient (PVU (100 km)$^{-1}$). Contours: White: PV on central isentrope, 2 PVU, black: standard deviation of wind speed on central isentrope, every 10 m s^{-1}, starting at 10 m s^{-1}.

https://doi.org/10.5194/egusphere-2024-1789
Preprint. Discussion started: 22 July 2024

the large case-by-case variability in the locations of enhanced precipitation associated with the frontal regions of low-pressure systems within each cluster. Variability is especially large for the precipitation upstream of the jet streak centre.

The variability in upper-level flow is smaller for clusters with fewer extreme events, compared to those with more extreme events, indicating a more variability for large-scale flow for stronger jet streaks (Compare upper two rows to the four lower rows in Figure F6). Finally, WCB outflow frequencies (Figure F7) are higher for extreme jet streak events for all clusters. The difference is most pronounce for the clusters with few extreme events.

Code and data availability. ERA5 reanalysis data can be downloaded from Hersbach et al. (2023).

Author contributions. Sebastian Schemm administered and supervised the work on this study and developed the concept and research questions together with Mona Bukenberger. Mona Bukenberger developed the methods, conducted data curation, analysis, and visualization. The manuscript was prepared by Mona Bukenberger, Sebastian Schemm, Stefan Rüdisühli, and Lena Fasnacht. Furthermore, Stefan Rüdisühli contributed to method development and visualisation, Lena Fasnacht to the methodology, and Nora Zillibotti to data curation and conceptualization.

Competing interests. At least one of the (co-)authors is a member of the editorial board of Weather and Climate Dynamics.

Acknowledgements. This research has been supported by the European Research Council, H2020 European Research Council (grant no. 848698). Two large language models have been used for the improvement of the quality and style of writing without any change in content, interpretation or meaning. The authors want to thank Dr. Alejandro Hermoso Verger and Dr. Katharina Heitmann for providing the Frame Jet regimes and WCB outflow masks, respectively. We also thank Dr. Hanna Joos and Dr. Franziska Aemisegger for fruitful discussions during early stages of the analysis, which helped to improve this work.

https://doi.org/10.5194/egusphere-2024-1789
Preprint. Discussion started: 22 July 2024

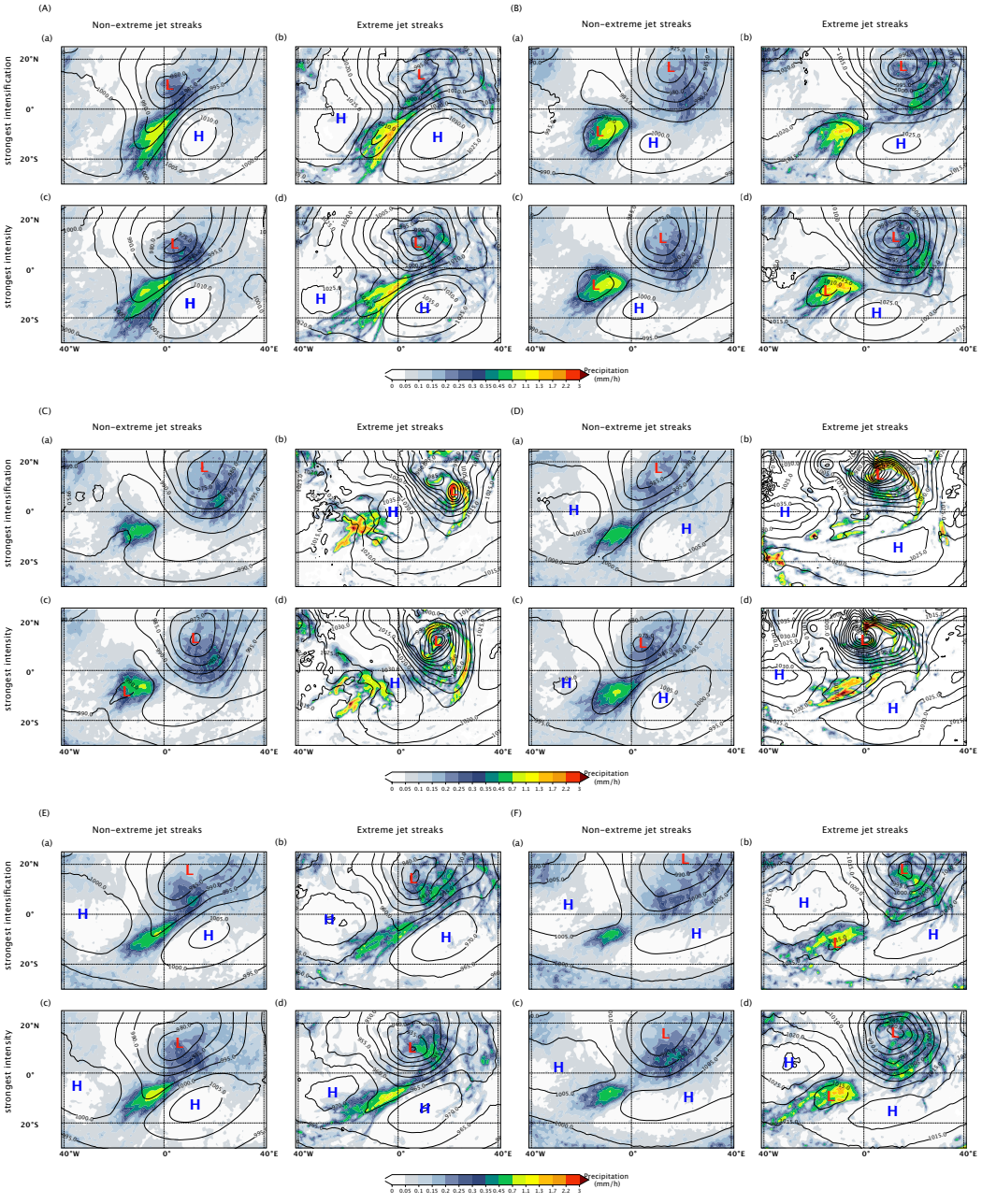

Figure F2. Jet streak centred composites. Colours: hourly precipitation. Contours: black: mean sea level pressure, every 5 hPa, starting at 970 hPa. As Fig. 16, but for jet streaks in Cluster 0 and 1 (top two rows), 2, 3 (middle two rows), and 4, 5 (lower two rows). Note that there are only two extreme events in C2 (left two columns in the middle two rows) and one extreme event in C3 (right two columns in the middle two rows).

https://doi.org/10.5194/egusphere-2024-1789
Preprint. Discussion started: 22 July 2024

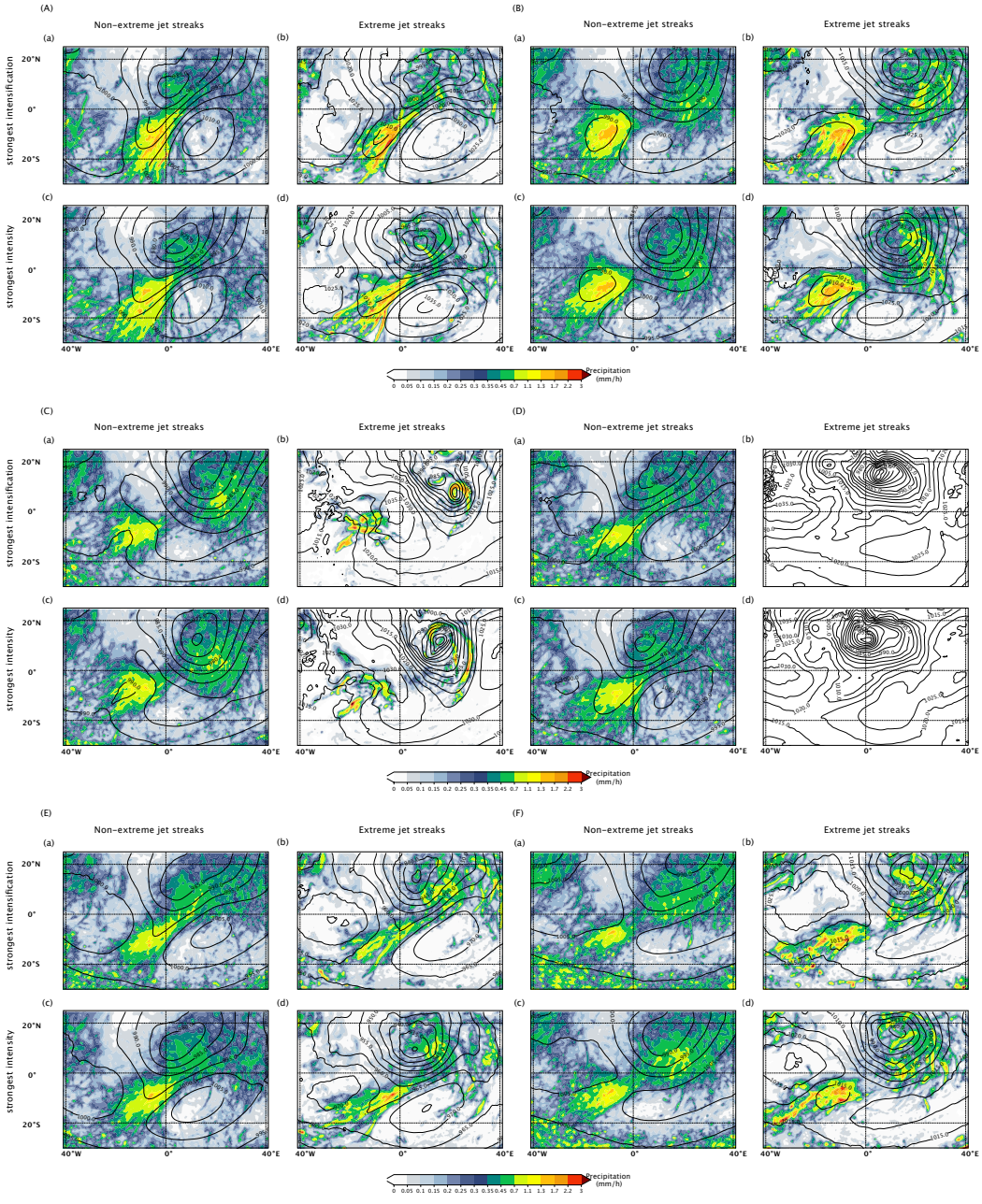

Figure F3. Jet streak centred composites. Colours: Standard deviation of hourly precipitation. Contours: black: mean sea level pressure, every 5 hPa, starting at 970 hPa. For Cluster 0 and 1 (top two rows), 2, 3 (middle two rows), and 4, 5 (lower two rows). Note that there are only two extreme events in C2 (left two columns in the middle two rows) and one extreme event in C3 (right two columns in the middle two rows).

https://doi.org/10.5194/egusphere-2024-1789
Preprint. Discussion started: 22 July 2024

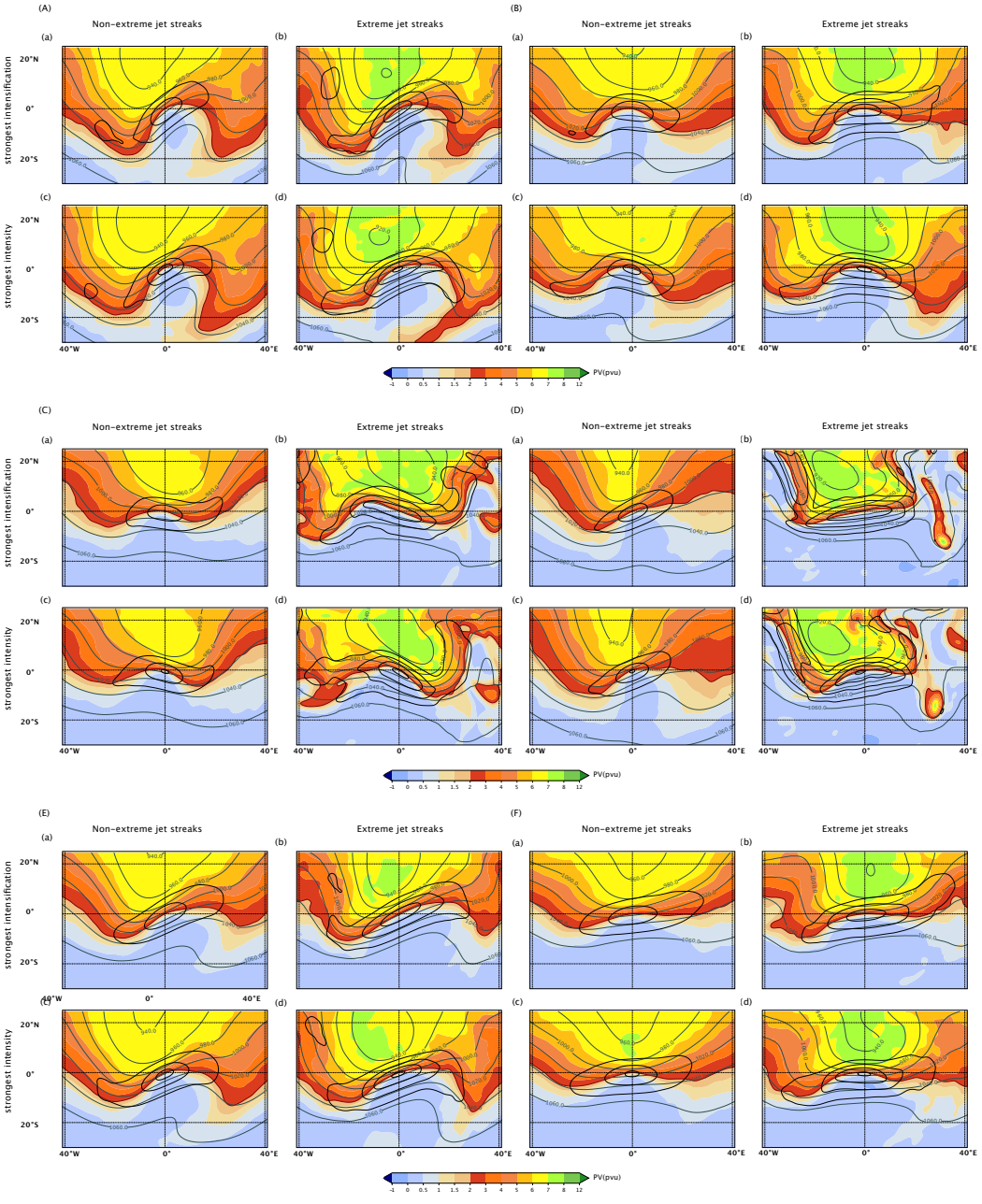

Figure F4. Jet streak centred composites. Colors: mean of PV on central jet streak isentrope, Contours: Dark grey: mean of geopotential height on 350 hPa pressure level, every 200 m, black: mean of wind speed on central isentrope, every 20 m s^{-1}, starting at 40 m s^{-1}. As Fig. 15, but for jet streaks in Cluster 0 and 1 (top two rows), 2, 3 (middle two rows), and 4, 5 (lower two rows). Note that there are only two extreme events in C2 (left two columns in the middle two rows) and one extreme event in C3 (right two columns in the middle two rows).

https://doi.org/10.5194/egusphere-2024-1789
Preprint. Discussion started: 22 July 2024

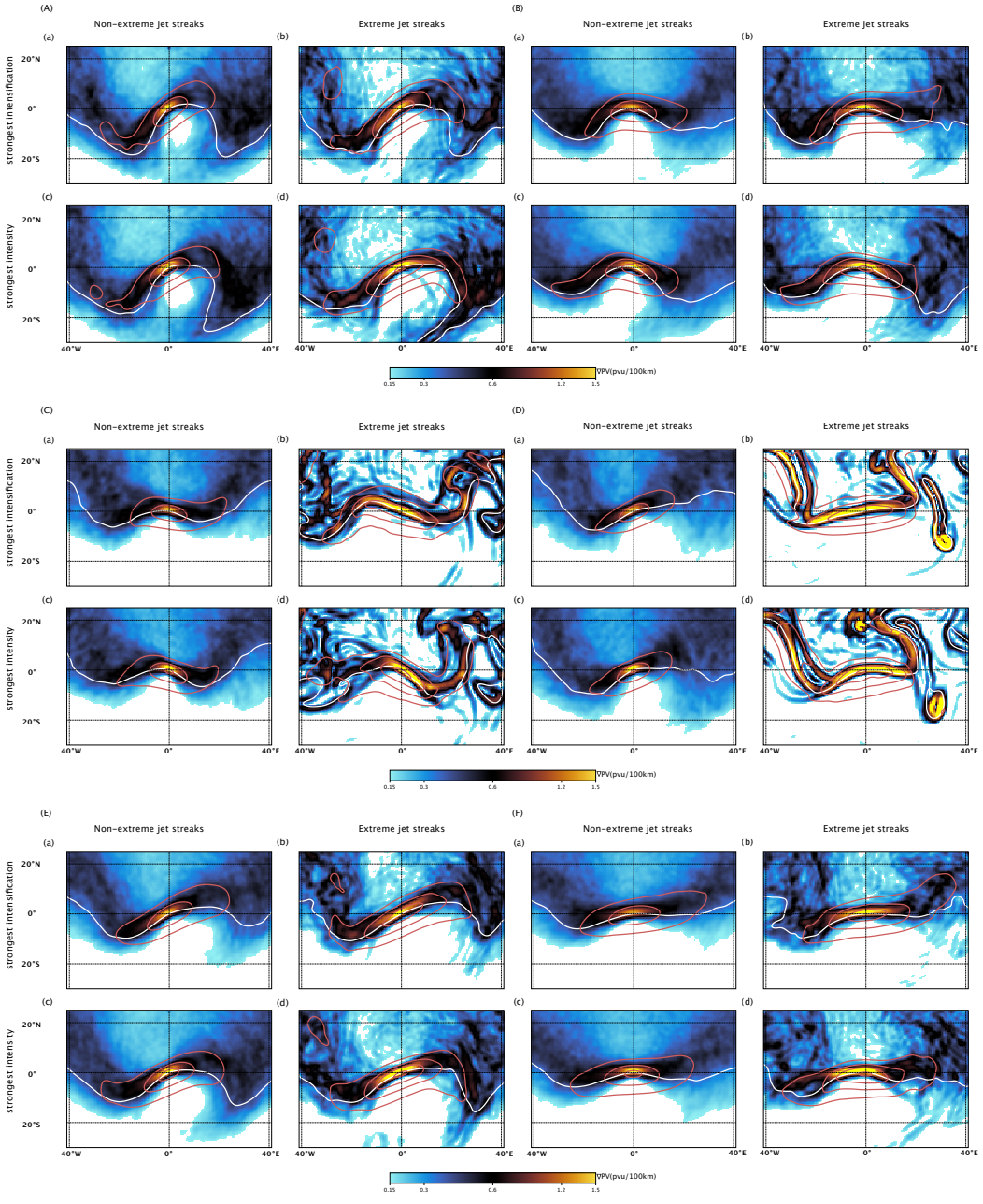

Figure F5. Jet streak centred composites. Colours: PV gradient (PVU (100 km)$^{-1}$), values smaller than 0.15 PVU (100 km)$^{-1}$ are white. Contours: White: PV on central isentrope, 2 PVU, red: wind speed on central isentrope, every 10 m s^{-1}, starting at 40 m s^{-1}. As Fig. 15, but for jet streaks in Cluster 0 and 1 (top two rows), 2, 3 (middle two rows), and 4, 5 (lower two rows). Note that there are only two extreme events in C2 (left two columns in the middle two rows) and one extreme event in C3 (right two columns in the middle two rows).

https://doi.org/10.5194/egusphere-2024-1789
Preprint. Discussion started: 22 July 2024

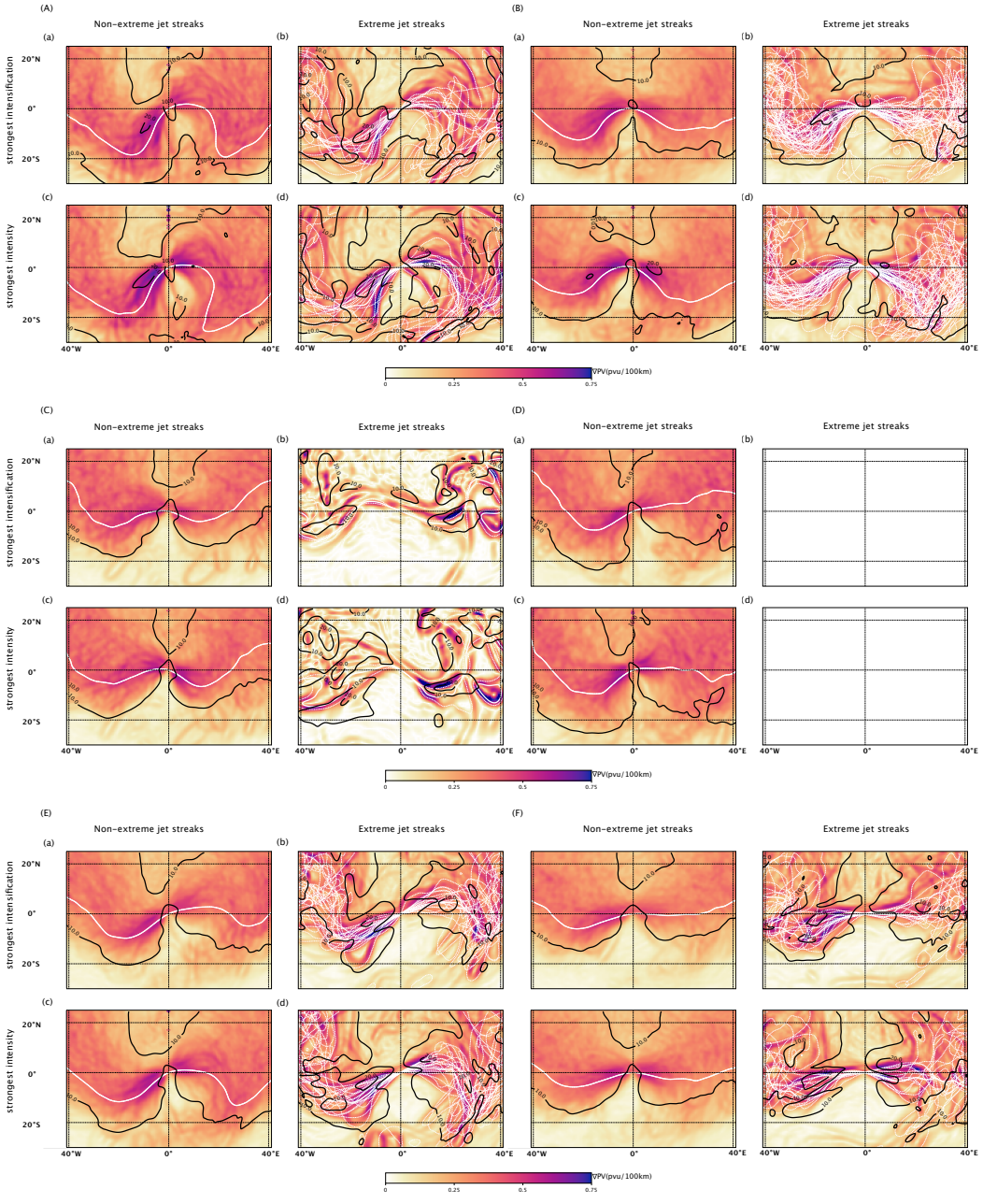

Figure F6. Jet streak centred composites based of, in Colours: standard deviation of PV gradient (PVU (100 km)$^{-1}$). Contours: White: PV on central isentrope, 2 PVU, black: standard deviation of wind speed on central isentrope, every 10 m s^{-1}, starting at 10 m s^{-1}. As Fig. F1, but for jet streaks in Cluster 0 and 1 (top two rows), 2, 3 (middle two rows), and 4, 5 (lower two rows). Note that there are only two extreme events in C2 (left two columns in the middle two rows) and one extreme event in C3 (right two columns in the middle two rows).

https://doi.org/10.5194/egusphere-2024-1789
Preprint. Discussion started: 22 July 2024

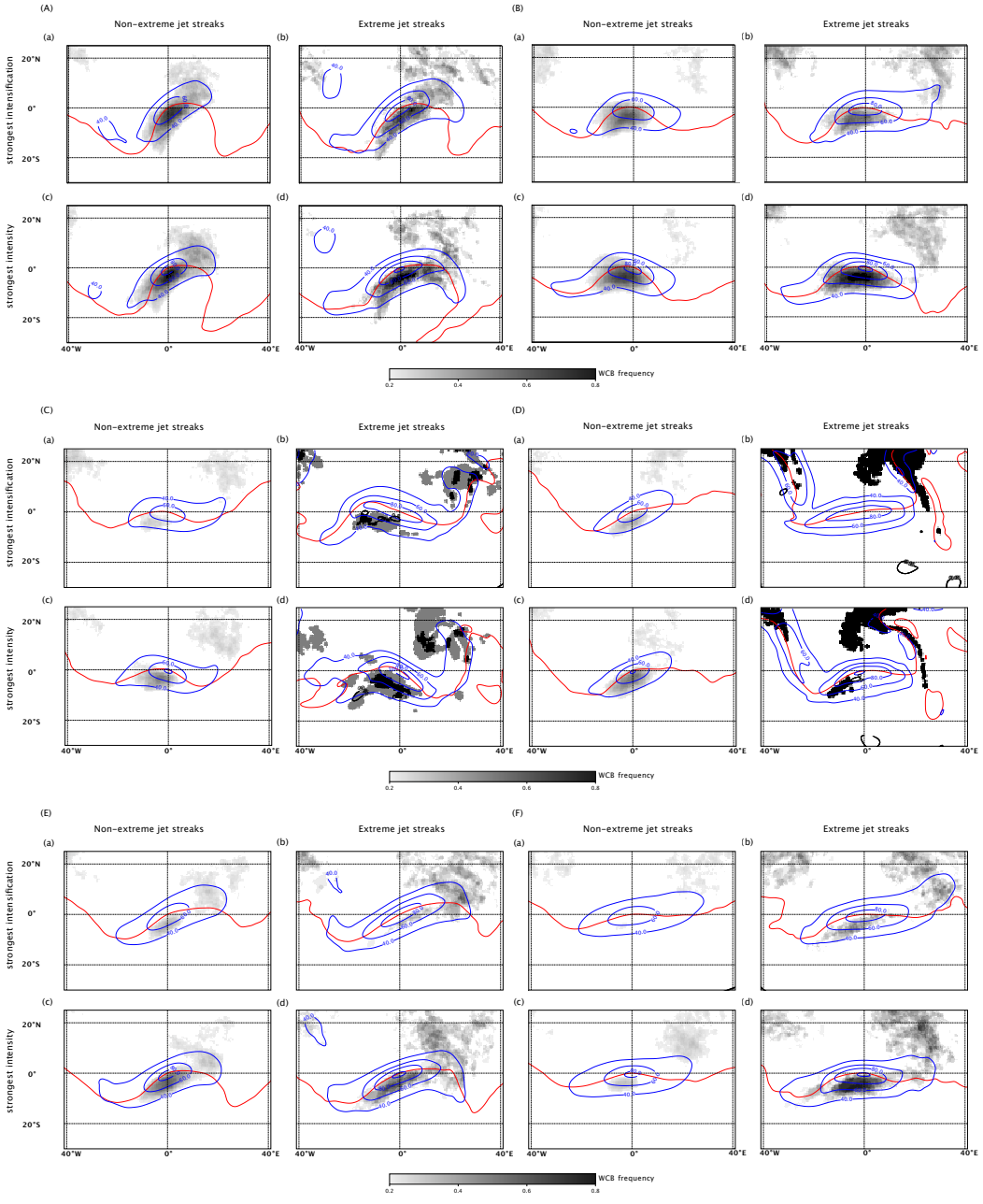

Figure F7. Jet streak centred composites. Colours: WCB outflow frequency on 500hPa. Contours: red: mean PV on central isentrope, 2 PVU, blue: mean of wind speed on central isentrope, every 20 m s^{-1}, starting at 40 m s^{-1}. As Fig. 17, but for jet streaks in Cluster 0 and 1 (top two rows), 2, 3 (middle two rows), and 4, 5 (lower two rows). Note that there are only two extreme events in C2 (left two columns in the middle two rows) and one extreme event in C3 (right two columns in the middle two rows).

https://doi.org/10.5194/egusphere-2024-1789
Preprint. Discussion started: 22 July 2024

References

Ambaum, M. H. P. and Novak, L.: A nonlinear oscillator describing storm track variability, Q. J. Roy. Meteor. Soc., 140, 2680–2684, https://doi.org/10.1002/qj.2352, 2014.

Armenakis, C. and Nirupama, N.: Urban impacts of ice storms: Toronto December 2013, Nat. Hazards., 74, 1291–1298, https://doi.org/10.1007/s11069-014-1211-7, 2014.

Attinger, R., Spreitzer, E., Boettcher, M., Wernli, H., and Joos, H.: Systematic assessment of the diabatic processes that modify low-level potential vorticity in extratropical cyclones, Weather Clim. Dynam., 2, 1073–1091, https://doi.org/10.5194/wcd-2-1073-2021, 2021.

Beebe, R. G. and Bates, F. C.: A Mechanism for Assisting in the Release of Convective Instability, Mon. Weather. Rev., 83, 1–10, https://doi.org/10.1175/1520-0493(1955)083<0001:AMFAIT>2.0.CO;2, 1955.

Benedict, J. J., Lee, S., and Feldstein, S. B.: Synoptic view of the North Atlantic oscillation, J. Atmos. Sci., 61, 121–144, https://doi.org/10.1175/1520-0469(2004)061<0121:SVOTNA>2.0.CO;2, 2004.

Binder, H., Boettcher, M., Joos, H., and Wernli, H.: The Role of Warm Conveyor Belts for the Intensification of Extratropical Cyclones in Northern Hemisphere Winter, J. Atmos. Sci., 73, 3997 – 4020, https://doi.org/10.1175/JAS-D-15-0302.1, 2016.

Bluestein, H. B. and Thomas, K. W.: Diagnosis of a Jet Streak in the Vicinity of a Severe Weather Outbreak in the Texas Panhandle, Mon. Weather. Rev., 112, 2499–2520, https://doi.org/10.1175/1520-0493(1984)112<2499:DOAJSI>2.0.CO;2, 1984.

Boyle, J. S. and Bosart, L. F.: Cyclone–Anticyclone Couplets over North America. Part II: Analysis of a Major Cyclone Event over the Eastern United States, Mon. Weather. Rev., 114, 2432 – 2465, https://doi.org/10.1175/1520-0493(1986)114<2432:CCONAP>2.0.CO;2, 1986.

Branstator, G. and Teng, H.: Tropospheric Waveguide Teleconnections and Their Seasonality, J. Atmos. Sci., 74, 1513 – 1532, https://doi.org/10.1175/JAS-D-16-0305.1, 2017.

Brayshaw, D. J., Hoskins, B., and Blackburn, M.: The Basic Ingredients of the North Atlantic Storm Track. Part I: Land–Sea Contrast and Orography, J. Atmos. Sci., 66, 2539 – 2558, https://doi.org/10.1175/2009JAS3078.1, 2009.

Bukenberger, M., Rüdisühli, S., and Schemm, S.: Jet stream dynamics from a potential vorticity gradient perspective: The method and its application to a kilometre-scale simulation, Q. J. Roy. Meteor. Soc., 149, 2409–2432, https://doi.org/10.1002/qj.4513, 2023.

Chang, E. K. M., Lee, S., and Swanson, K. L.: Storm Track Dynamics, J. Climate, 15, 2163–2183, https://doi.org/10.1175/1520-0442(2002)015<02163:STD>2.0.CO;2, 2002.

Clark, A. J., Schaffer, C. J., Gallus, W. A., and Johnson-O'Mara, K.: Climatology of Storm Reports Relative to Upper-Level Jet Streaks, Weather Forecast., 24, 1032–1051, https://doi.org/10.1175/2009WAF2222216.1, 2009.

Cunningham, P. and Keyser, D.: Analytical and numerical modelling of jet streaks: Barotropic dynamics, Q. J. Roy. Meteor. Soc., 126, 3187–3217, https://doi.org/10.1002/qj.49712657010, 2000.

Cunningham, P. and Keyser, D.: Dynamics of jet streaks in a stratified quasi-geostrophic atmosphere: Steady-state representations, Q. J. Roy. Meteor. Soc., 130, 1579–1609, https://doi.org/10.1256/qj.03.35, 2004.

Davies, H.: Emergence of the mainstream cyclogenesis theories, Meteorologische Z., 6, 261–274, https://doi.org/10.1127/metz/6/1997/261, 1997.

Davies, H. C. and Didone, M.: Diagnosis and dynamics of forecast error growth, Mon. Weather. Rev., 141, 2483–2501, https://doi.org/10.1175/MWR-D-12-00242.1, 2013.

https://doi.org/10.5194/egusphere-2024-1789
Preprint. Discussion started: 22 July 2024

Davies, H. C. and Rossa, A. M.: PV Frontogenesis and Upper-Tropospheric Fronts, Mon. Weather. Rev., 126, 1528 – 1539, https://doi.org/10.1175/1520-0493(1998)126<1528:PFAUTF>2.0.CO;2, 1998.

Davis, C. A. and Emanuel, K. A.: Potential Vorticity Diagnostics of Cyclogenesis, Mon. Weather. Rev., 119, 1929 – 1953, https://doi.org/10.1175/1520-0493(1991)119<1929:PVDOC>2.0.CO;2, 1991.

Eichelberger, S. J. and Hartmann, D. L.: Zonal Jet Structure and the Leading Mode of Variability, J. Climate, 20, 5149–5163, https://doi.org/10.1175/JCLI4279.1, 2007.

Ertel, H. and Rossby, C.: A new conservation theorem of Hydrodynamics, Q. J. Roy. Meteor. Soc., 1942.

Frame, T. H. A., Ambaum, M. H. P., Gray, S. L., and Methven, J.: Ensemble prediction of transitions of the North Atlantic eddy-driven jet, Q. J. Roy. Meteor. Soc., 137, 1288–1297, https://doi.org/10.1002/qj.829, 2011.

Gentleman, R.: Cophenetic Distances for a Hierarchical Clustering, https://stat.ethz.ch/R-manual/R-devel/library/stats/html/cophenetic.html, last opened on 06.06.2024, 2023.

Grams, C. M., Wernli, H., Böttcher, M., Čampa, J., Corsmeier, U., Jones, S. C., Keller, J. H., Lenz, C.-J., and Wiegand, L.: The key role of diabatic processes in modifying the upper-tropospheric wave guide: a North Atlantic case-study, Q. J. Roy. Meteor. Soc., 137, 2174–2193, https://doi.org/10.1002/qj.891, 2011.

Gray, S. L., Dunning, C., Methven, J., Masato, G., and Chagnon, J. M.: Systematic model forecast error in Rossby wave structure, Geophys. Res. Lett., 41, 2979–2987, https://doi.org/10.1002/2014GL059282, 2014.

Gyakum, J. R.: On the Evolution of the QE II Storm. I: Synoptic Aspects, Mon. Weather. Rev., 111, 1137 – 1155, https://doi.org/10.1175/1520-0493(1983)111<1137:OTEOTI>2.0.CO;2, 1983.

Harnik, N., Galanti, E., Martius, O., and Adam, O.: The anomalous merging of the African and North Atlantic jet streams during the Northern Hemisphere winter of 2010, J. Climate, 27, 7319–7334, https://doi.org/10.1175/JCLI-D-13-00531.1, 2014.

Hartmann, D. L.: The Atmospheric General Circulation and Its Variability, J. Meterol. Soc. Jpn., 85B, 123–143, https://doi.org/10.2151/jmsj.85B.123, 2007.

Hersbach, H. and Bell, B. e. a.: The ERA5 global reanalysis, Q. J. Roy. Meteor. Soc., 146, 1999–2049, https://doi.org/10.1002/qj.3803, 2020.

Hersbach, H., Bell, B., Berrisford, P., Biavati, G., Horányi, A., Muñoz Sabater, J., Nicolas, J., Peubey, C., Radu, R., Rozum, I., Schepers, D., Simmons, A., Soci, C., Dee, D., and Thépaut, J.-N.: ERA5 hourly data on pressure levels from 1940 to present, Tech. rep., Climate Change Service (C3S) Climate Data Store (CDS), https://doi.org/10.24381/cds.bd0915c6, 2023.

Hewitson, B. and Crane, R.: Self-Organizing Maps: Applications to synoptic climatology, Clim. Res., 22, 13–26, https://doi.org/10.3354/cr022013, 2002.

Hoskins, B. and Berrisford, P.: A potential vorticity perspective of the storm of 15–16 October 1987, Weather, 43, 122–129, https://doi.org/10.1002/j.1477-8696.1988.tb03890.x, 1988.

Hoskins, B. J., James, I. N., and White, G. H.: The Shape, Propagation and Mean-Flow Interaction of Large-Scale Weather Systems, J. Atmos. Sci., 40, 1595–1612, https://doi.org/10.1175/1520-0469(1983)040<1595:TSPAMF>2.0.CO;2, 1983.

Hoskins, B. J., McIntyre, M. E., and Robertson, A. W.: On the use and significance of isentropic potential vorticity maps, Q. J. Roy. Meteor. Soc., 111, 877–946, https://doi.org/10.1002/qj.49711147002, 1985.

Jain, A. K.: Data clustering: 50 years beyond K-means, Pattern Recognition Letters, 31, 651–666, https://doi.org/10.1016/j.patrec.2009.09.011, 2010.

Karnauskas, K. B., Donnelly, J. P., Barkley, H. C., and Martin, J. E.: Coupling between air travel and climate, Nat. Clim. Change, 5, 1068–1073, https://doi.org/10.1038/nclimate2715, 2015.

https://doi.org/10.5194/egusphere-2024-1789
Preprint. Discussion started: 22 July 2024

Kiviluoto, K.: Topology preservation in self-organizing maps, in: Proceedings of International Conference on Neural Networks (ICNN'96), vol. 1, pp. 294–299 vol.1, https://doi.org/10.1109/ICNN.1996.548907, 1996.

Koch, P., Wernli, H., and Davies, H. C.: An event-based jet-stream climatology and typology, Int. J. Climatol., 26, 283–301, https://doi.org/10.1002/joc.1255, 2006.

Kohonen, T.: Self-Organizing Maps, Springer Berlin, Heidelberg, https://doi.org/10.1007/978-3-642-97610-0, 1995.

Lane, T. P., Sharman, R. D., Trier, S. B., Fovell, R. G., and Williams, J. K.: Recent Advances in the Understanding of Near-Cloud Turbulence, B. Am. Meterol. Soc., 93, 499–515, https://doi.org/10.1175/BAMS-D-11-00062.1, 2012.

Li, C. and Wettstein, J. J.: Thermally driven and eddy-driven jet variability in reanalysis, J. Climate, 25, 1587–1596, https://doi.org/10.1175/JCLI-D-11-00145.1, 2012.

Liu, Y. and Weisberg, R. H.: A Review of Self-Organizing Map Applications in Meteorology and Oceanography, in: Self Organizing Maps, edited by Mwasiagi, J. I., chap. 13, IntechOpen, Rijeka, https://doi.org/10.5772/13146, 2011.

Manola, I., Selten, F., de Vries, H., and Hazeleger, W.: "Waveguidability" of idealized jets, J. Geophys. Res.-Atmos., 118, 10,432–10,440, https://doi.org/10.1002/jgrd.50758, 2013.

Martius, O., Schwierz, C., and Davies, H. C.: Tropopause-Level Waveguid, J. Atmos. Sci., 67, 866–879, https://doi.org/10.1175/2009JAS2995.1, 2010.

Martínez-Alvarado, O., Madonna, E., Gray, S. L., and Joos, H.: A route to systematic error in forecasts of Rossby waves, Q. J. Roy. Meteor. Soc., 142, 196–210, https://doi.org/10.1002/qj.2645, 2016.

Namias, J. and Clapp, P. F.: Confluence Theory of the High Tropospheric Jet Stream, J. Atmos. Sci., 6, 330–336, https://doi.org/10.1175/1520-0469(1949)006<0330:CTOTHT>2.0.CO;2, 1949.

Palmén, E. H. and Newton, C. W.: Atmospheric circulation systems: their structure and physical interpretation, vol. 13, Academic press, 1969.

Pedregosa, F., Varoquaux, G., Gramfort, A., Michel, V., Thirion, B., Grisel, O., Blondel, M., Prettenhofer, P., Weiss, R., Dubourg, V., Vanderplas, J., Passos, A., Cournapeau, D., Brucher, M., Perrot, M., and Duchesnay, E.: Scikit-learn: Machine Learning in Python, J. Mach. Learn. Res., 12, 2825–2830, 2011.

Pfahl, S., Schwierz, C., Croci-Maspoli, M., Grams, C. M., and Wernli, H.: Importance of latent heat release in ascending air streams for atmospheric blocking, Nat. Geosci., 8, 610–614, https://doi.org/10.1038/ngeo2487, 2015.

Polster, C. and Wirth, V.: A New Atmospheric Background State to Diagnose Local Waveguidability, Geophys. Res. Lett., 50, e2023GL106 166, https://doi.org/10.1029/2023GL106166, 2023.

Reiter, E. R. and Nania, A.: Jet-Stream Structure and Clear-Air Turbulence (CAT), Journal of Applied Meteorology and Climatology, 3, 247–260, https://doi.org/10.1175/1520-0450(1964)003<0247:JSSACA>2.0.CO;2, 1964.

Riehl, H.: Jet stream in upper troposphere and cyclone formation, Eos, Transactions American Geophysical Union, 29, 175–186, https://doi.org/10.1029/TR029i002p00175, 1948.

Riehl, H. and Sidney Teweles, J.: A Further Study on the Relation between the Jet Stream and Cyclone Formation, 5, 66, https://doi.org/10.3402/tellusa.v5i1.8561, 1953.

Rivière, G.: A Dynamical Interpretation of the Poleward Shift of the Jet Streams in Global Warming Scenarios, J. Atmos. Sci., 68, 1253–1272, https://doi.org/10.1175/2011JAS3641.1, 2011.

https://doi.org/10.5194/egusphere-2024-1789
Preprint. Discussion started: 22 July 2024

Rose, S. F., Hobbs, P. V., Locatelli, J. D., and Stoelinga, M. T.: A 10-Yr Climatology Relating the Locations of Reported Tornadoes to the Quadrants of Upper-Level Jet Streaks, Weather Forecast., 19, 301–309, https://doi.org/10.1175/1520-0434(2004)019<0301:AYCRTL>2.0.CO;2, 2004.

Saffin, L., Gray, S. L., Methven, J., and Williams, K. D.: Processes Maintaining Tropopause Sharpness in Numerical Models, J. Geophys. Res.-Atmos., 122, 9611–9627, https://doi.org/10.1002/2017JD026879, 2017.

Saffin, L., Methven, J., Bland, J., Harvey, B., and Sanchez, C.: Circulation conservation in the outflow of warm conveyor belts and consequences for Rossby wave evolution, Q. J. Roy. Meteor. Soc., 147, 3587–3610, https://doi.org/10.1002/qj.4143, 2021.

Sanders, F. and Bosart, L. F.: Mesoscale Structure in the Megalopolitan Snowstorm of 11–12 February 1983. Part I: Frontogenetical Forcing and Symmetric Instability, J. Atmos. Sci., 42, 1050–1061, https://doi.org/10.1175/1520-0469(1985)042<1050:MSITMS>2.0.CO;2, 1985.

Schemm, S. and Wernli, H.: The Linkage between the Warm and the Cold Conveyor Belts in an Idealized Extratropical Cyclone, J. Atmos. Sci., 71, 1443 – 1459, https://doi.org/10.1175/JAS-D-13-0177.1, 2014.

Schemm, S., Wernli, H., and Papritz, L.: Warm Conveyor Belts in Idealized Moist Baroclinic Wave Simulations, J. Atmos. Sci., 70, 627 – 652, https://doi.org/10.1175/JAS-D-12-0147.1, 2013.

Schemm, S., Rivière, G., Ciasto, L. M., and Li, C.: Extratropical cyclogenesis changes in connection with tropospheric ENSO teleconnections to the North Atlantic: Role of stationary and transient waves, J. Atmos. Sci., 75, 3943–3964, https://doi.org/10.1175/JAS-D-17-0340.1, 2018.

Schulzweida, U.: CDO User Guide, https://doi.org/10.5281/zenodo.10020800, 2023.

Shaw, T. A. and Miyawaki, O.: Fast upper-level jet stream winds get faster under climate change, Nat. Clim. Change, pp. 1–7, https://doi.org/10.1038/s41558-023-01884-1, 2023.

Steinfeld, D., Boettcher, M., Forbes, R., and Pfahl, S.: The sensitivity of atmospheric blocking to upstream latent heating – numerical experiments, Weather Clim. Dynam., 1, 405–426, https://doi.org/10.5194/wcd-1-405-2020, 2020.

Storer, L. N., Williams, P. D., and Joshi, M. M.: Global Response of Clear-Air Turbulence to Climate Change, Geophys. Res. Lett., 44, 9976–9984, https://doi.org/10.1002/2017GL074618, 2017.

Thorncroft, C. D., Hoskins, B. J., and McIntyre, M. E.: Two paradigms of baroclinic-wave life-cycle behaviour, Q. J. Roy. Meteor. Soc., 119, 17–55, https://doi.org/10.1002/qj.49711950903, 1993.

Uccellini, L. W.: The Coupling of Upper and Lower Tropospheric Jet Streaks and Implications for the Development of Severe Convective Storms, University of Wisconsin–Madison, google-Books-ID: 1aPVAAAAMAAJ, 1977.

Uccellini, L. W. and Kocin, P. J.: The Interaction of Jet Streak Circulations during Heavy Snow Events along the East Coast of the United States, Weather Forecast., 2, 289–308, https://doi.org/10.1175/1520-0434(1987)002<0289:TIOJSC>2.0.CO;2, 1987.

Uccellini, L. W., Kocin, P. J., Petersen, R. A., Wash, C. H., and Brill, K. F.: The Presidents' Day Cyclone of 18–19 February 1979: Synoptic Overview and Analysis of the Subtropical Jet Streak Influencing the Pre-Cyclogenetic Period, Mon. Weather. Rev., 112, 31–55, https://doi.org/10.1175/1520-0493(1984)112<0031:TPDCOF>2.0.CO;2, 1984.

Velden, C. S. and Mills, G. A.: Diagnosis of Upper-Level Processes Influencing an Unusually Intense Extratropical Cyclone over Southeast Australia, Weather Forecast., 5, 449–482, https://doi.org/10.1175/1520-0434(1990)005<0449:DOULPI>2.0.CO;2, 1990.

Vesanto, J., Himberg, J., and Alhoniemi, E.: SOM Toolbox for Matlab 5, WorkingPaper Report A57, 2000.

Ward, J. H.: Hierarchical Grouping to Optimize an Objective Function, J. Am. Stat. Assoc., 58, 236–244, https://doi.org/10.1080/01621459.1963.10500845, 1963.

https://doi.org/10.5194/egusphere-2024-1789
Preprint. Discussion started: 22 July 2024

Wernli, H., Dirren, S., Liniger, M. A., and Zillig, M.: Dynamical aspects of the life cycle of the winter storm 'Lothar' (24–26 December 1999), Q. J. Roy. Meteor. Soc., 128, 405–429, https://doi.org/10.1256/003590002321042036, 2002.

Williams, P. D.: Transatlantic flight times and climate change, Environ. Res. Lett., 11, 024 008, https://doi.org/10.1088/1748-9326/11/2/024008, 2016.

Williams, P. D.: Increased light, moderate, and severe clear-air turbulence in response to climate change, Adv. Atmos. Sci., 34, 576–586, https://doi.org/10.1007/s00376-017-6268-2, 2017.

Williams, P. D. and Joshi, M. M.: Intensification of winter transatlantic aviation turbulence in response to climate change, Nat. Clim. Change, 3, 644–648, https://doi.org/10.1038/nclimate1866, 2013.

Winters, A. C.: Kinematic processes contributing to the intensification of anomalously strong North Atlantic jets, Q. J. Roy. Meteor. Soc., 147, 2506–2532, https://doi.org/10.1002/qj.4037, 2021.

Wirth, V.: Waveguidability of idealized midlatitude jets and the limitations of ray tracing theory, Weather Clim. Dynam., 1, 111–125, https://doi.org/10.5194/wcd-1-111-2020, 2020.

Woollings, T., Hoskins, B., Blackburn, M., and Berrisford, P.: A New Rossby Wave–Breaking Interpretation of the North Atlantic Oscillation, J. Atmos. Sci., 65, 609–626, https://doi.org/10.1175/2007JAS2347.1, 2008.

Woollings, T., Hannachi, A., and Hoskins, B.: Variability of the North Atlantic eddy-driven jet stream, Q. J. Roy. Meteor. Soc., 136, 856–868, https://doi.org/10.1002/qj.625, 2010.